minerals

MDPI

Article

Source Rock Evaluation and Hydrocarbon Expulsion Characteristics of Effective Source Rocks in the Fushan Depression, Beibuwan Basin, China

Xirong Wang [1,2], Fujie Jiang [1,2,*], Xiaowei Zheng [1,2], Di Chen [1,2], Zhenguo Qi [1,2], Yilin Liu [1,2], Jing Guo [1,2] and Yuqi Zhang [1,2]

[1] State Key Laboratory of Petroleum Resources and Engineering, China University of Petroleum (Beijing), Beijing 102249, China; wxr940831@163.com (X.W.); zhengxiaowei1103@outlook.com (X.Z.); cd18801323769@163.com (D.C.); qizhg7@126.com (Z.Q.); 2022020015@cugb.edu.cn (Y.L.); 2023310032@student.cup.edu.cn (J.G.); m13840642098@163.com (Y.Z.)

[2] College of Geosciences, China University of Petroleum (Beijing), Beijing 102249, China

* Correspondence: jfjhtb@163.com

Abstract: This study presents an integrated approach using organic geochemistry and incident-light organic petrographic microscopy techniques to characterize the kerogen type, hydrocarbon potential, thermal maturity, and effective depositional environment of the Eocene Liushagang Formation intervals in the western Huangtong Sag, eastern Bailian Sag, central Huachang Sub-uplift, and Southern Slope Zone area in the Fushan Depression, Beibuwan Basin. The results show that the hydrocarbon potential of these organic-rich lacustrine shale areas is mainly dependent on the depositional environment and the present-day burial depth of sediments. Oscillations and transitions between (i) rocks with dominant allochthonous organic matter (including primary/reworked vitrinite and inertinite macerals and terrestrial debris particles) representing a large influence of continental sediments (e.g., source supply direction) and (ii) rocks with dominant autochthonous organic matter (e.g., alginite) indicate a distal and stable lacustrine basin depositional environment. The source rock thickness ranges from 40.1 to 387.4 m. The average TOC of the Liushagang Formation in the Fushan Sag is between 0.98% and 2.00%, with the highest organic matter abundance being in the first and second sections of the Liushagang Formation, presenting as high-quality source rocks. The organic matter is predominantly Type II_1 and Type II_2. The highest vitrinite reflectance (1.14%) is in the Huangtong and Bailian Sags. The source rocks of the second section of the Liushagang Formation are primary hydrocarbon generators, contributing 55.11% of the total generation. Hydrocarbon sequestration peaks at %Ro 0.80%, with a maximum efficiency of 97.7%. The cumulative hydrocarbon generation of the Liushagang Formation is 134.10×10^8 tons, with 50.52×10^8 tons having been expelled and 83.58×10^8 tons remaining. E_2L_{2X} and E_2L_{2S} have maximum hydrocarbon displacement intensities of 184.22×10^4 t/km² and 45.39×10^4 t/km², respectively, with cumulative displacements of 52.99×10^8 tons and 15.58×10^8 tons. The oil and gas accumulation system is highly prospective, showing significant exploration potential.

Keywords: Liushagang Formation; source rock evaluation; hydrocarbon expulsion; Fushan Depression

Citation: Wang, X.; Jiang, F.; Zheng, X.; Chen, D.; Qi, Z.; Liu, Y.; Guo, J.; Zhang, Y. Source Rock Evaluation and Hydrocarbon Expulsion Characteristics of Effective Source Rocks in the Fushan Depression, Beibuwan Basin, China. *Minerals* **2024**, *14*, 975. https://doi.org/10.3390/min14100975

Academic Editor: Thomas Gentzis

Received: 5 August 2024
Revised: 22 September 2024
Accepted: 23 September 2024
Published: 27 September 2024

1. Introduction

The Beibuwan Basin, an oil- and gas-rich sedimentary basin on the northern margin of the South China Sea, has a proven geological reserve of crude oil of approximately 4.05×10^8 t and a proven geological reserve of natural gas of approximately 50×10^8 m^3 [1–3]. Although its petroleum exploration started in 1965, early research focused on the structural analysis of the Beibuwan Basin [4–7]. In 1977, the first well in the Beibuwan Basin was drilled, showing that the Palaeogene Liushagang Formation (E_2L) had

good source rocks, and the industrial oil flow was tested in the third member of the Liushagang Formation (E_2L_3) [8]. After that, the source rock evaluation in the Beibuwan Basin started to gain increasing attention, and it is believed that the source rocks of the Paleogene Liushagang Formation function as the main source rocks in the Beibuwan Basin [9–12], However, since there are multiple sets of source rocks, like seven sub-members of the Liushagang Formation that have developed in the depression [13–15], the quality and hydrocarbon seepage characteristics are still unclear. This has limited the understanding of the resource potential and the selection of favorable resource fields.

The major hydrocarbon-producing source rocks in the Beibuwan Basin include the Weixinan Depression, Wushi Depression, Maichen Depression, Fushan Depression, and Haizhong Depression [16–19], among which the Fushan Depression, located on the southern margin of the Beibuwan Basin, has turned out to be a new oil-producing block, demonstrating proven geological reserves of oil of about 3139.41 $\times$ 10^4 t and proven geological reserves of natural gas of 123.87 $\times$ 10^8 m^3 by the end of 2021 [13,20,21]. Therefore, this small, but abundant, oil- and gas-rich sag has received a lot of attention from the industry [22], and the hydrocarbon generation and expulsion characteristics of the source rocks of the Liushagang Formation (E_2L_3, E_2L_2, and E_2L_1) in the Fushan Depression should be evaluated systematically and analyzed thoroughly.

As the amount of hydrocarbon generation and expulsion from source rocks determines the calculation of the amount of hydrocarbon that can be extracted [23–27], it is of significance to understand the evaluation scheme of the source rocks and the potential of the oil and gas resources [28–33]. Therefore, the current widely applied calculation methods for evaluating hydrocarbon expulsion are the diffusion hydrocarbon expulsion mode, fluid seepage method, simulation experiment method, and hydrocarbon expulsion threshold method [34–37], among which there is not much agreement [26,38–40]. This could be explained by the limitations of these methods. For example, only light hydrocarbons are involved in diffusion throughout the hydrocarbon migration process. Therefore, the diffusion hydrocarbon expulsion model is only suitable for guiding natural gas-related migration simulation [41]. The critical saturation of hydrocarbon seepage from the source rock is the same as the factors influencing the oil seepage concentration. Hence, a variation profile can be established according to the principle of two-phase seepage to perform analogy analysis [42]. The hydrocarbon expulsion from the thermal simulation method can provide parameters for calculating the resource quantity. But, the obtained hydrocarbon production rate is not accurate enough [43]. Therefore, this work selected the source rocks of the Liushagang Formation in the Fushan Depression for a comprehensive evaluation of source rocks, simulating the hydrocarbon generation and expulsion characteristics of the source rocks and calculating the amount of oil and gas from different accumulation systems. This study will deepen the understanding of the source rocks in the Fushan Depression, thus providing a reference for the further study of oil and gas migration and accumulation in the Fushan Depression and a scientific basis for the further exploration and development of the study area.

2. Geological Setting

2.1. Tectonic Setting

The Fushan Depression has a total area of 2920 km^2 and is located on the southern margin of the Beibuwan Basin on the continental shelf of the South China Sea and the slope of the Haizhong uplift. The shape of the nearly triangular depression in the Fushan Depression is closely related to the left-lateral strike-slip of the NW-trending Red River Fault and the clockwise rotation of the Palaeogene Hainan Island [11,44–46]. On the western side, it is adjacent to the Lingao uplift, and on the eastern side, the Yunlong uplift is visible [45,47]. The Shenhu movement at the end of the Late Cretaceous formed a series of NE-trending faults and rifts [48,49]. It was controlled by the Cenozoic regional tectonic deformation of the northern continental margin of the South China Sea, and a series of NE-trending faults and small fault structures developed in the Beibuwan Basin during this period [50,51].

The Lingao Fault and Yunlong Fault control the area, forming a superimposed depression, which includes several small adjustment faults, including the Meihua Fault and the Lianhua Fault. This geological arrangement results in a pattern of alternating [52,53]. In the northern sector of the Meihua Fault, the following significant deep sag regions are discernible: the Huangtong Sag to the west and the Bailian Sag to the east. Sandwiched between these sags lies the central interval structural transformation zone, known as the Huachang Sub-uplift. Collectively, these features delineate the northern deep concave area. Conversely, the area situated to the south of the Meihua Fault is characterized by the Southern Slope Belt [54,55] (Figure 1).

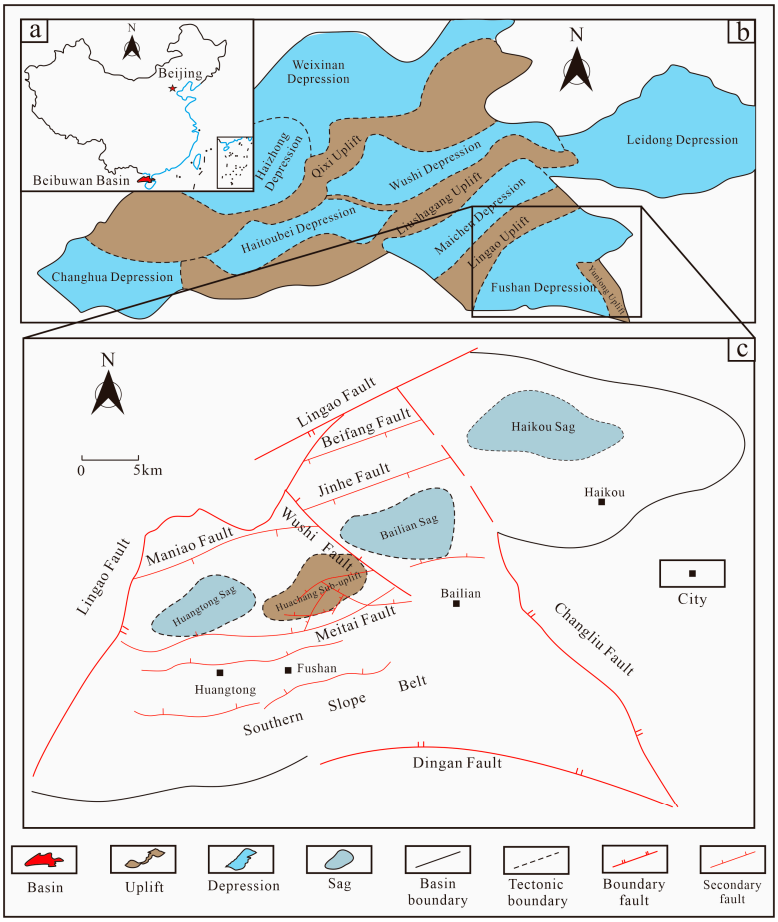

Figure 1. (**a**) Location of the Beibuwan Basin. (**b**) Location of the Fushan Depression (modified after [56]). (**c**) Location of western Huangtong Sag, eastern Bailian Sag, central Huachang Sub-uplift, and Southern Slope Belt in the Fushan Depression (modified after [57]).

2.2. Sedimentology

The Palaeogene Changliu Formation, Liushagang Formation, and Weizhou Formation, along with Neogene and Quaternary sediments, have been sequentially deposited upon the Cretaceous basement in the Fushan Depression. Notably, the Liushagang Formation, characterized by its lacustrine deltaic deposits, serves as the principal source of oil and a key reservoir within the Fushan Depression [58,59]. The Eocne Liushagang Formation was categorized into three members in this area, namely, E_2L_1, E_2L_2, and E_2L_3. It is divided into E_2L_{3X}, E_2L_{3Z}, E_2L_{3S}, E_2L_{2X}, E_2L_{2S}, E_2L_{1X}, and E_2L_{1S} sequentially, and hydrocarbon source rocks are developed in these layers [60], among which E_2L_1 and the E_2L_3 are the main oil- and gas-producing layers [13] (Figure 2). The boreholes examined in this study are predominantly located in the onshore regions of structural highs, encompassing the sedimentary core of the western Huangtong Sag, the central Huachang Sub-uplift, and the elevated Southern Slope Belt [61,62]. The objective is to ascertain the distribution and

stratigraphic variations in the source rocks within the onshore areas. Controlled by the Meihua fault, E_2L_3 in the eastern Huangtong Sag is denuded. The northern sea area is the subsidence center of the Bailian Sag in the northeast. The distribution range of the non-well area is wide, and the basic data on lithology and layer thickness are lacking [3].

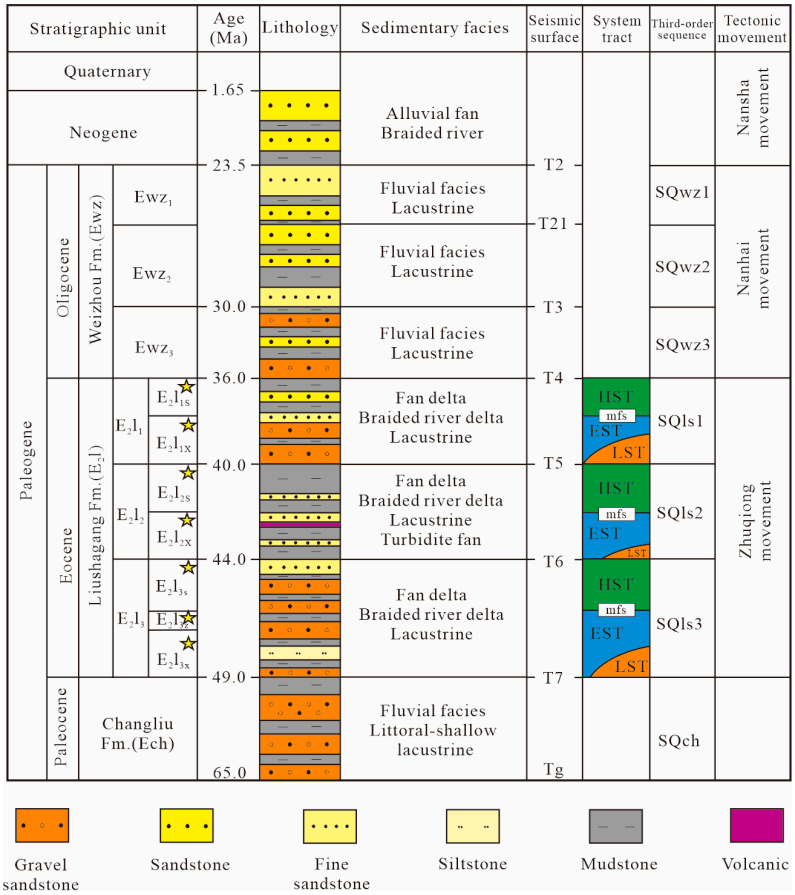

Figure 2. Stratigraphic column of the Fushan Depression (modified after [13]). E_2L_1, E_2L_2, and E_2L_3 are Members 1, 2, and 3 of the Eocne Liushagang Formation. According to the lithological characteristics and the production demand of China's oil fields, it is divided into the E_2L_{3X}, E_2L_{3Z}, E_2L_{3S}, E_2L_{2X}, E_2L_{2S}, E_2L_{1X}, and E_2L_{1S} sequentially from the top to bottom of Eocene source rocks.

3. Methods and Workflows

3.1. Samples

This study meticulously analyzed 119 sediment samples from 65 wells located in the Fushan Depression. The spatial distribution of samples from the Liushagang Formation within this depression exhibits a pronounced and discernible pattern. The wells were categorized into two distinct regions as follows: the Huantong Sag in the west and the Bailian Sag in the east of the Fushan Depression (Figure 3). Core observations, total organic carbon (TOC) analysis, rock pyrolysis, bitumen extraction (extracted bitumen A), and vitrinite reflectance measurements were conducted on a total of 119 samples. These analyses were performed to evaluate the quality of the primary source rock intervals (E_2L_{3X}, E_2L_{3Z}, E_2L_{3S}, E_2L_{2X}, E_2L_{2S}, $E_2L_{1X,}$ and E_2L_{1S}) of the Liushagang Formation. Simultaneously, the threshold for hydrocarbon displacement was ascertained to differentiate between effective and ineffective source rocks.

3.2. Laboratory Methods

The abundance, type, and thermal maturity of organic matter in source rocks are important factors in assessing the hydrocarbon generation capacity of source rocks in

sedimentary basins. Leco CS230 and Rock-Eval 2 pyrolysis analyses, as per the methodology [63], were conducted to ascertain the total organic carbon (TOC), temperature of maximum hydrocarbon generation (Tmax), thermally extractable HCs (S_1), and remaining HC generating potential (S_2) content. In the context of the HAWK pyrolysis analysis, the samples underwent initial pyrolysis at 300 °C for 3 min, followed by a ramping rate of 25 °C per minute up to a final temperature of 650 °C. The liberated hydrocarbons were quantified as S_1 and S_2 employing a Flame Ionization Detector (FID). The data about TOC, S_1, and S_2 exhibited an accuracy and precision exceeding 95%, and the Tmax determination was accurate to within ±2 °C. These assessments were validated through the analysis of standard reference materials, which encompass Chinese standard reference materials [64,65].

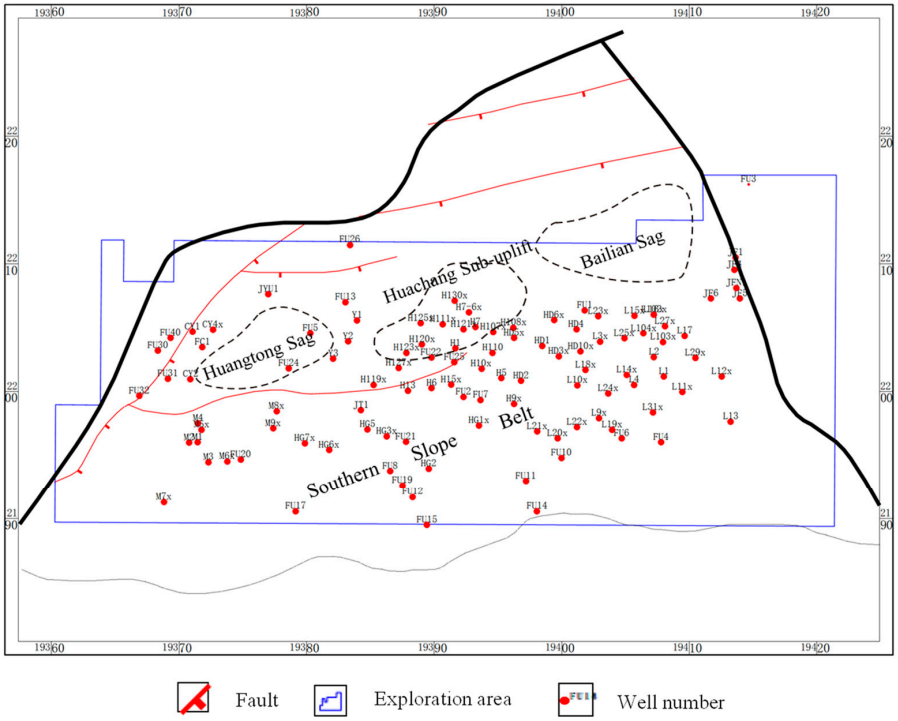

Figure 3. Sample position distribution in the Liushagang Formation in Fushan Depression. The wells in the west of the study area, such as *FC1*, were assigned to the Huantong Sag. The *L* well in the east belongs to the Bailian area, which is assigned to the Bailian Sag. The wells in the central turning zone north of the Meihua Fault are classified into the Huachang Sub-uplift, and the wells north of the Meihua Fault are located in the Southern Slope Belt.

Maceral identification such as the sapropel group, quantitative counting, and vitrinite reflectance (*Ro*, %) measurements were also conducted in this work. The samples were sectioned either perpendicularly or parallel to the bedding planes and subsequently processed in accordance with the guidelines outlined in [66]. Reflectance assessments were conducted using a Leica 4500 P microscope (Wetzlar, Germany), developed by Leica Company in Germany, equipped with a CRAIC microscope photometer or a Leica DM4 M microscope, both of which were integrated with a Hilgers Technisches Büro Fossil system. These systems were furnished with both white and ultraviolet light sources, adhering to the standards set forth in [67,68]. Random reflectance (Rr) measurements were executed utilizing an oil immersion objective lens with a 50× magnification. The infrared spectral parameters of kerogen, Tmax from pyrolysis, and vitrinite reflectance (*Ro*, %) were all used in this work to identify the degree of thermal evolution of organic matter. In addition, vitrinite reflectance was used as a determination index to establish the fitting relationship with burial depth to determine the maturity characteristics of organic matter in the target horizon of the study area.

3.3. Hydrocarbon Generation and Expulsion Conceptual Model

This study employed PetroMod. V9.0 software, developed by the IES Company in Germany, to simulate the burial, hydrocarbon generation, and thermal histories of key individual wells within the Fushan Depression. Specifically, Yong 7 well in the western region and Lian 23 well in the eastern region were selected for detailed single-well simulation analysis (Figure 3).

The hydrocarbon generation and expulsion conceptual model is a systematic method for analyzing the effectiveness of source rocks. The hydrocarbon generation potential index $(S_1 + S_2)/TOC$ represents the hydrocarbon generation potential per unit of organic matter. It increases with Ro during the evolutionary process until it reaches the current maximum hydrocarbon generation potential index ($HCIo$). Following that, the cumulative hydrocarbon generation equals the residual hydrocarbon saturation of the source rock, which is the limit at which the hydrocarbon generation potential index begins to decrease and the source rock begins to expel hydrocarbons [36,69].

The key procedures for establishing the source rock hydrocarbon generation and expulsion model [70] using the hydrocarbon generation potential are as below:

(1) Establishment of the hydrocarbon generation potential profile: The pyrolysis database of source rocks in the study area was set up. The profile of the hydrocarbon generation potential index with vitrinite reflectance or burial depth of source rocks in the study area was made determined on the data.

(2) Calculation of the hydrocarbon expulsion rate: After determining the hydrocarbon generation and expulsion threshold of the study area according to the establishment of the step (1) handle, HCI_o and HCI_P were brought into Equation (2), which was used to calculate μ, which was then brought into Equation (3), and the HCI'_o corresponding to any point on the evolution profile of hydrocarbon generation potential index were calculated in batches. The hydrocarbon expulsion rates $q_e(Z)$ corresponding to different depths Z were determined.

$$q_e(Z) = HCI'_o(Z) - HCI_P(Z) \quad (1)$$

$$\mu = (1 - 0.083 \times HCI_P) / (1 - 0.083 \times HCI_o) \quad (2)$$

$$HCI'_o = \mu \times HCI_o \quad (3)$$

where Z represents different depths. HCI_o is the hydrocarbon generation potential index corresponding to the hydrocarbon expulsion threshold of the maximum current hydrocarbon generation potential. HCI_P is the actual hydrocarbon generation potential index. μ is the restitution coefficient of the hydrocarbon generation potential index. HCI'_o is the maximum original hydrocarbon generation potential. $q_e(Z)$ is the hydrocarbon expulsion rate corresponding to Z.

(3) Calculation of hydrocarbon expulsion intensity: $q_e(Z)$ calculated in step (2) and H, Z, and the organic carbon mass fraction of the source rock corresponding to different burial depths Z were introduced into Equation (4).

$$E_{hc} = \int_{Z_0}^{Z} q_e(Z) \times H \times \rho(Z) \times \mathrm{TOC} \times \mathrm{d}Z \quad (4)$$

where H and $\rho(Z)$ are the rock thickness and density, among which Z_0 represents the hydrocarbon expulsion threshold of the study horizon. The final integral operation is the hydrocarbon expulsion intensity E_{hc} with a unit of 10^3 t/km^2.

(4) Calculation of the hydrocarbon expulsion rate: The hydrocarbon expulsion rate was defined as the change in the hydrocarbon expulsion rate in the unit thermal evolution degree [71,72].

$$V_e = \Delta q_e / \Delta R_o \quad (5)$$

where V_e is the hydrocarbon expulsion rate, Δq_e is the hydrocarbon expulsion rate difference of adjacent data points, and ΔR_o is the vitrinite reflectance difference and R_o.

(5) Calculation of the hydrocarbon expulsion efficiency: The ratio of hydrocarbon expulsion to cumulative production at a certain point can be replaced by the proportion of the difference between HCI'_o and HCI_o in HCI'_o. By bringing the relevant parameters obtained in Equation (2) into Equation (6), R_{eo} was calculated [73].

$$R_{eo} = q_e(Z)/HCI'_o(Z) \times 100\% \quad (6)$$

where R_{eo} is the hydrocarbon removal efficiency at a given point.

(6) Calculation of the amount of hydrocarbon expulsion: According to Equation (3), E_{hc} and the other parameters required for the calculation, such as $S(n)$, were put into Equation (7) for integral operation and to determine the amount of Q_e.

$$Q_e = \int_1^n 10^{-3} \times E_{hc} \times S(n) \times \mathrm{d}n \quad (7)$$

where $S(n)$ is the unit area of the source rock and Q_e is the hydrocarbon expulsion in each sedimentary period of the study area that can be obtained.

4. Geochemical Characteristics of Eocene Source Rocks

4.1. Organic Matter Abundance

Based on total organic carbon (TOC) measurements, and hydrocarbon source rock extracts, and applying the established criteria for lacustrine mudstone abundance in China, the regions of elevated TOC within E_2L_3 are predominantly localized in the Bailian Sag and the Southern Slope Belt. E_2L_{3X} is classified within the medium source rock category, exhibiting a comparatively lower concentration of organic matter in comparison with the other constituent sub-segments. E_2L_{3Z} and E_2L_{3S} belong to the range of good source rocks, and the abundance of organic matter is higher. The high TOC value of E_2L_2 is mainly in the Huangtong Sag and Bailian Sag, and the organic matter abundance is better than that of other layers. The organic matter abundance of E_2L_{2X} and E_2L_{2S} is higher, and the hydrocarbon generation potential is up to 19.79 mg/g. The high-value area is located in the western Huangtong Sag, with an average value of 3.64 mg/g, which has great hydrocarbon generation potential and is a good source of rock with high quality. The TOC value of E_2L_1 is highest in the two hydrocarbon generation centers, Huangtong Sag and Bailian Sag, and decreases towards the edge of the Huachang Sub-uplift and Southern Slope Belts. The organic matter abundance of E_2L_{1X} and E_2L_{1S} is high, which belongs to the range of good source rocks (Table 1, and Figures 4–6).

Table 1. The organic matter abundance of the source rocks of the Liushagang Formation and the Fushan Depression.

Characteristics		TOC/wt %		Extracted Bitumen "A"/%		S_1+S_2/(mg HC/g Rocks)	
		Distribution	Samples	Distribution	Samples	Distribution	Samples
E_2L_{1S}	Huangtong Sag	0.52~1.9 0.91	24	0.014~0.117 0.068	12	0.33~4.52 2.11	11
	Source rock evaluation	Medium		Medium		Medium	
	Bailian Sag	0.64~1.36 1.03	9	0.031~0.19 0.088	4	0.98~3.92 2.55	4
	Source rock evaluation	Good		Medium		Medium	

Table 1. *Cont.*

Characteristics		TOC/wt %		Extracted Bitumen "A"/%		S_1+S_2/(mg HC/g Rocks)	
		Distribution	Samples	Distribution	Samples	Distribution	Samples
E_2L_{1X}	Huangtong Sag	0.67~3.61 1.40	36	0.025~0.32 0.091	33	1.38~8.43 3.07	30
	Source rock evaluation	Good		Medium		Medium	
	Bailian Sag	0.48~1.75 1.30	9	0.042~0.107 0.078	3	1.46~3.49 2.75	3
	Source rock evaluation	Good		Medium		Medium	
E_2L_{2S}	Huangtong Sag	0.77~3.04 1.46	42	0.013~0.363 0.102	30	1.4~7.17 3.78	40
	Source rock evaluation	Good		Good		Medium	
	Bailian Sag	0.49~1.86 1.49	10	0.0242~0.1335 0.0739	5	0.5~3.04 1.62	5
	Source rock evaluation	Good		Medium		Poor	
E_2L_{2X}	Huangtong Sag	-	-	-	-	-	-
	Source rock evaluation	-		-		-	
	Bailian Sag	0.16~2.45 1.61	44	0.008~0.245 0.114	31	0.08~7.67 3.17	35
	Source rock evaluation	Good		Good		Medium	
E_2L_{3S}	Huangtong Sag	-	-	-	-	-	-
	Source rock evaluation	-		-		-	
	Bailian Sag	0.44~1.89 1.40	13	0.073~0.172 0.121	5	1.88~4.62 2.67	5
	Source rock evaluation	Good		Good		Medium	
E_2L_{3X}	Huangtong Sag	1.14	1	0.0607	1	2.78	1
	Source rock evaluation	Good		Medium		Medium	
	Bailian Sag	-	-	-	-	-	-
	Source rock evaluation	-		-		-	

4.2. Kerogen Type

The hydrogen index (*HI*) and Tmax were used to identify the organic matter type. The results show that E_2L_{3X} is mainly II_2 and III in the Southern Slope Belt, while the kerogen type of E_2L_{3Z} changed from II_1 in the Meihua Fault to II_2 and III in the Southern Slope Belt. During the deposition of E_2L_{3S}, the kerogen of the Huachang Sub-uplift was type II_2 and type II_1, the kerogen of the Huangtong Sag was type II_2, and the kerogen of the Southern Slope Belt was type II_2 and type III. The kerogen types of the Huachang Sub-uplift in the E_2L_{2X} depositional period were type II_1 and type II_2. The kerogen type of the Huangtong Sag is mainly type II_2 but some are type II_1 and type III. The kerogen type of E_2L_{2S} transits from type II_1 to type III from west to east, and all three types of kerogens are found in the Southern Slope Belt. The organic matter type of E_2L_{1X} transits from type II_1 to type II_2 from west to east, and the Southern Slope Belt is dominated by type II_2 kerogen, followed by type III. The northern part of E_2L_{1S} is type II_2 kerogen, and type III kerogen occurs in the Southern Slope Belt (Figure 7).

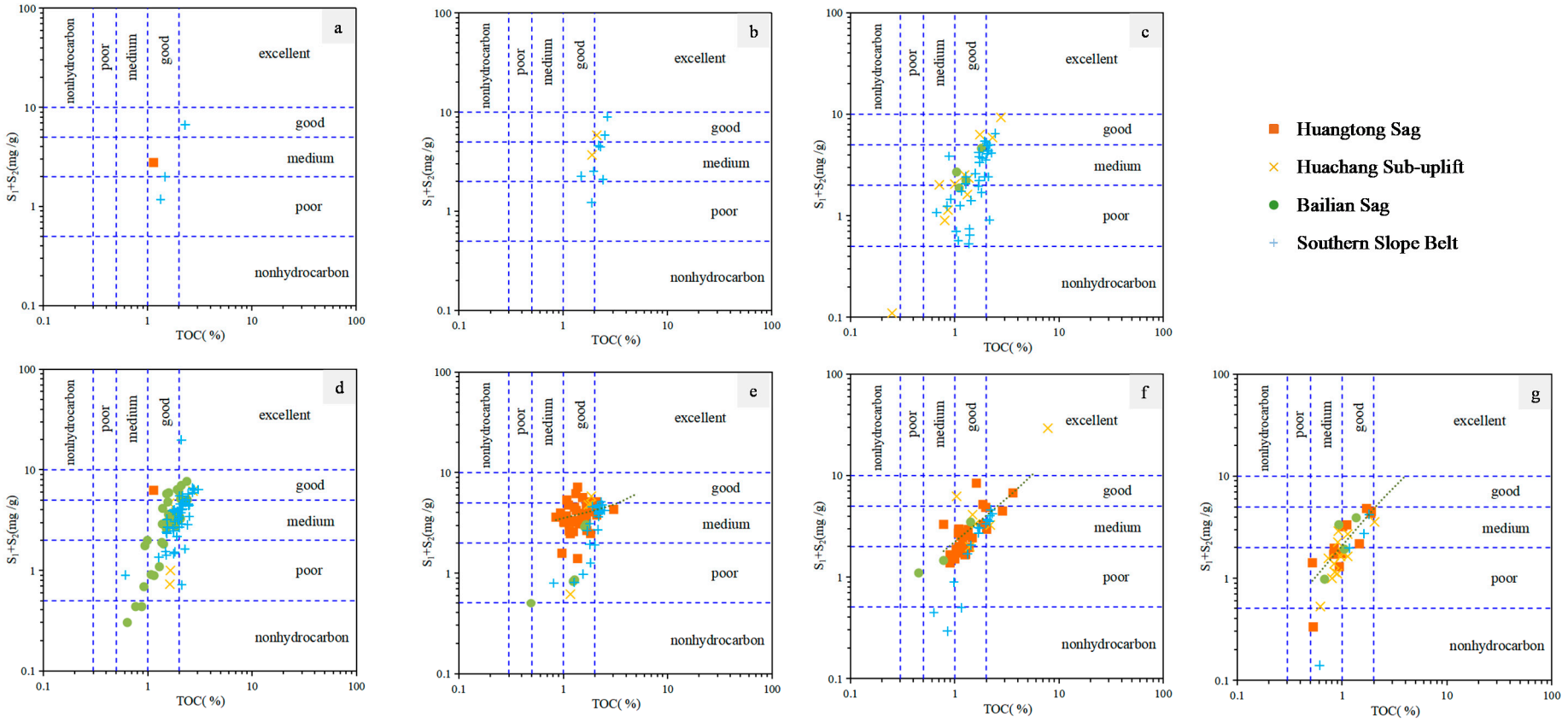

Figure 4. Relationship between total organic carbon content and hydrocarbon generation potential of source rocks in the Huangtong Sag, Huachang Sub-uplift, Bailian Sag, and Southern Slope Belt in the Fushan Depression. The E_2L_{2X} stratigraphic sub-section exhibits superior geological parameters compared with its counterparts, indicating significant hydrocarbon generation potential. (**a**) E_2L_{3X} source rocks; (**b**) E_2L_{3Z} source rocks; (**c**) E_2L_{3S} source rocks; (**d**) E_2L_{2X} source rocks; (**e**) E_2L_{2S} source rocks (**f**) E_2L_{1X} source rocks; and (**g**) E_2L_{1S} source rocks (after [74]).

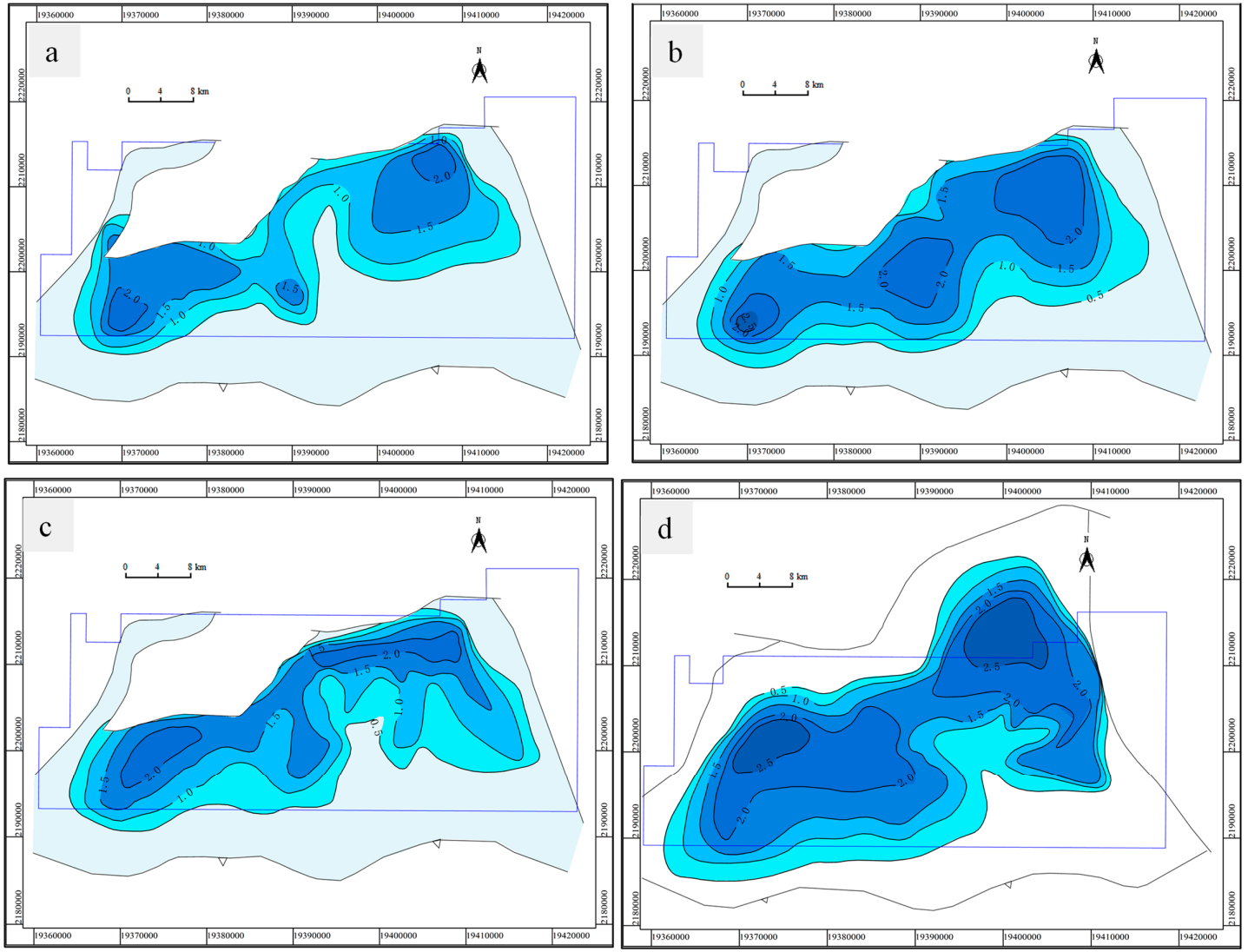

Figure 5. *Cont.*

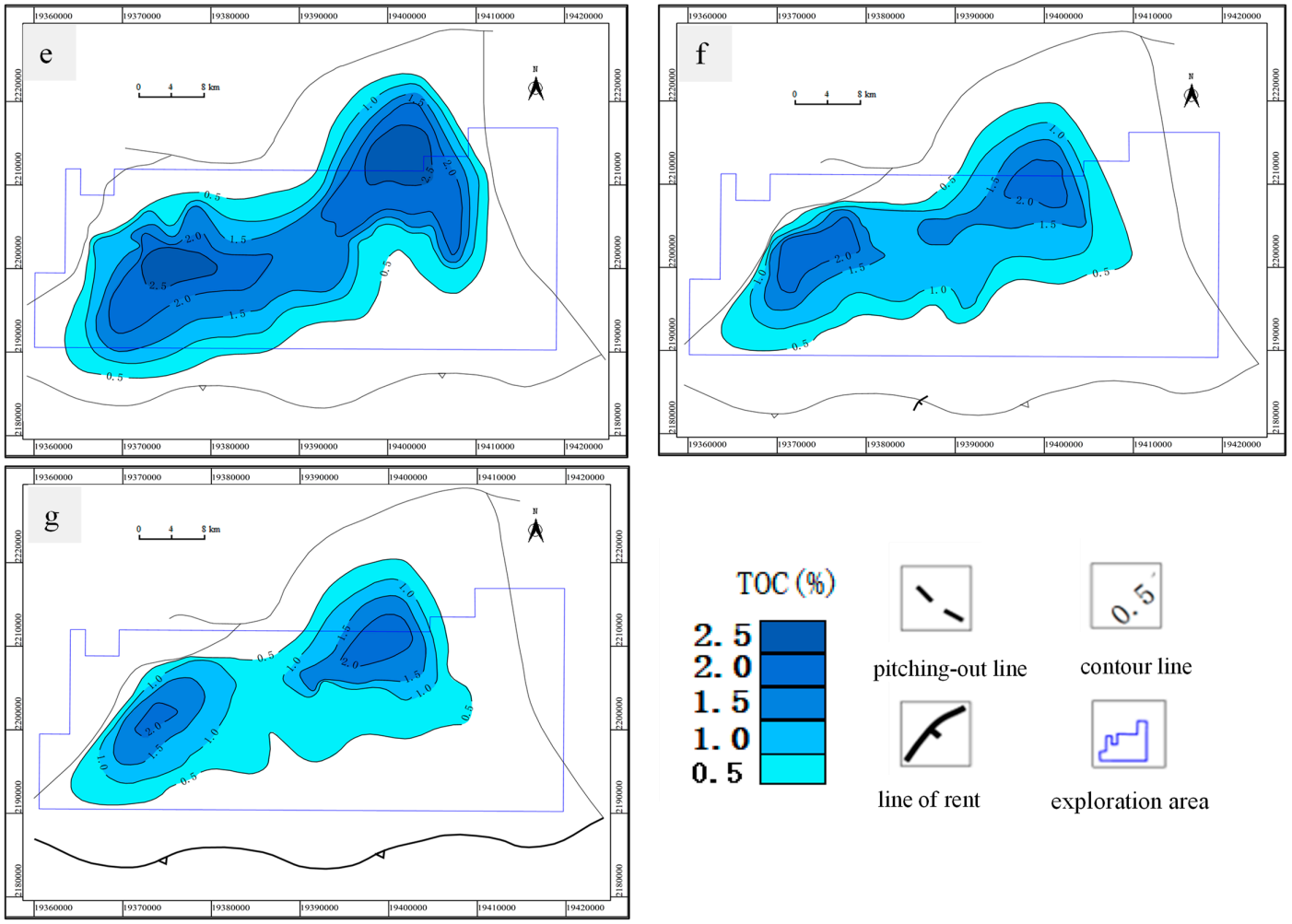

Figure 5. TOC contour map of the Liuliushagang Formation in the Fushan Depression. The TOC content ranges from 0.5% to 3.6%, indicating a substantial abundance of organic matter. The elevated concentrations are predominantly found within the Huangtong and Bailian Sag regions, with a gradual decrease towards the peripheral areas. The E_2L_{2X} and E_2L_{2S} strata exhibit superior characteristics compared with the other geological layers. (**a**) E_2L_{3X} source rocks; (**b**) E_2L_{3Z} source rocks; (**c**) E_2L_{3S} source rocks; (**d**) E_2L_{2X} source rocks; (**e**) E_2L_{2S} source rocks; (**f**) E_2L_{1X} source rocks; and (**g**) E_2L_{1S} source rocks.

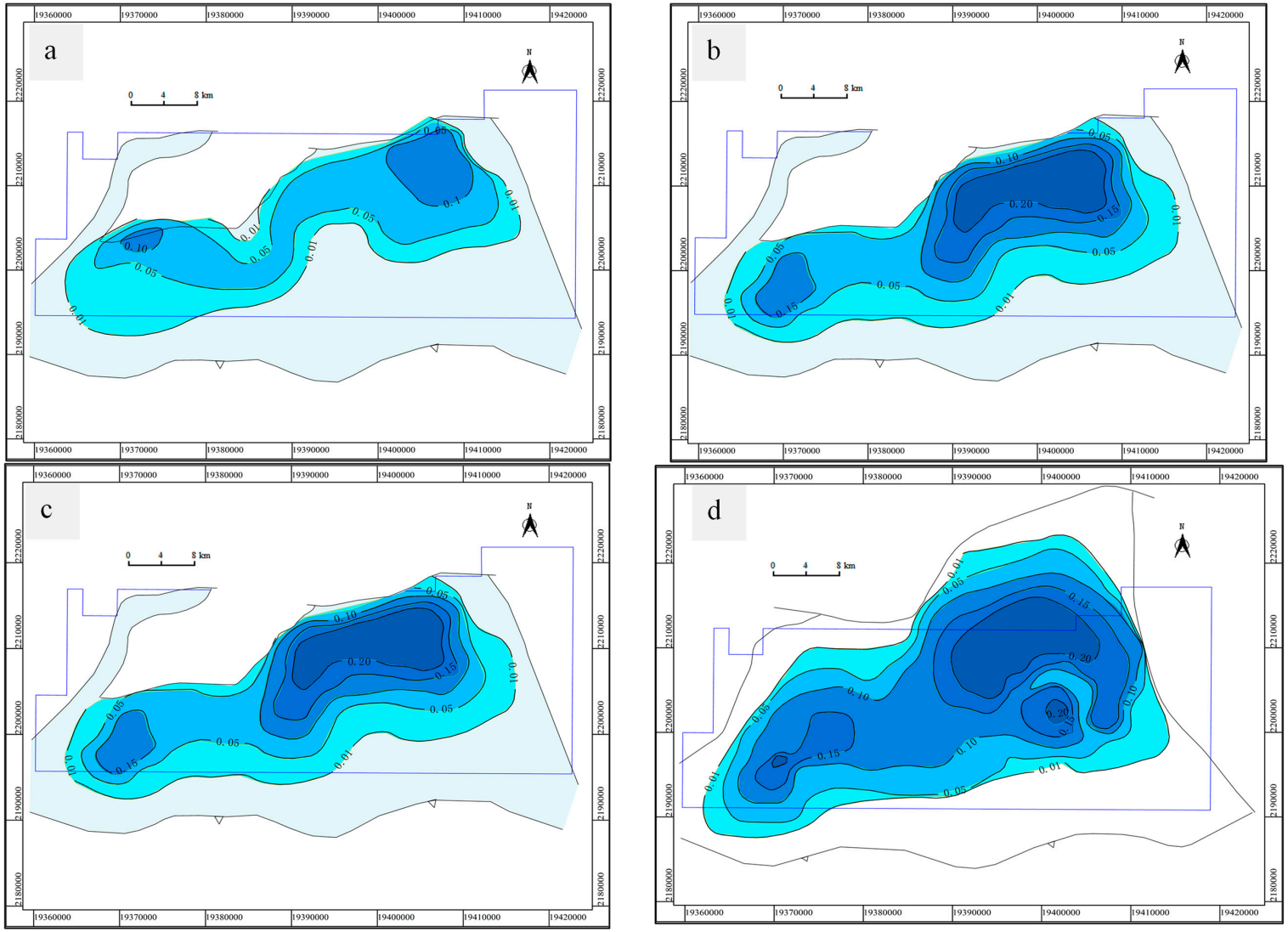

Figure 6. *Cont.*

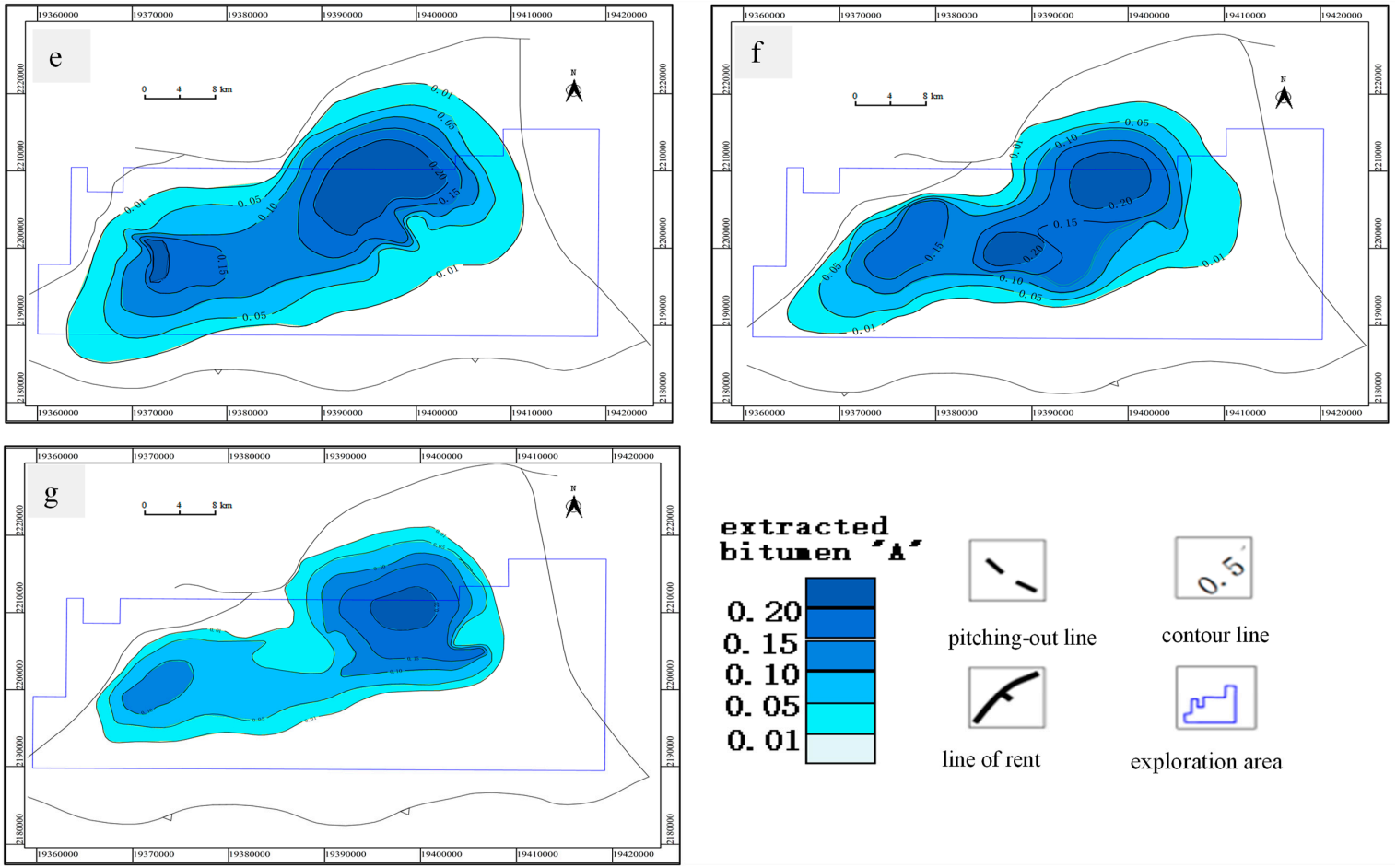

Figure 6. Extracted bitumen *A* contour map of the Liushagang Formation in the Fushan Depression. The extracted bitumen A content ranges from 0.01% to 0.54%, indicating a substantial organic matter abundance. The highest concentrations are predominantly found within the Bailian Sag, while the Huachang Sub-uplift exhibits elevated values in the E_2L_{2X} and E_2L_{2S} intervals, as well as in the E_2L_{1X} stratigraphic unit. (**a**) E_2L_{3X} source rocks; (**b**) E_2L_{3Z} source rocks; (**c**) E_2L_{3S} source rocks; (**d**) E_2L_{2X} source rocks; (**e**) E_2L_{2S} source rocks; (**f**) E_2L_{1X} source rocks; and (**g**) E_2L_{1S} source rocks.

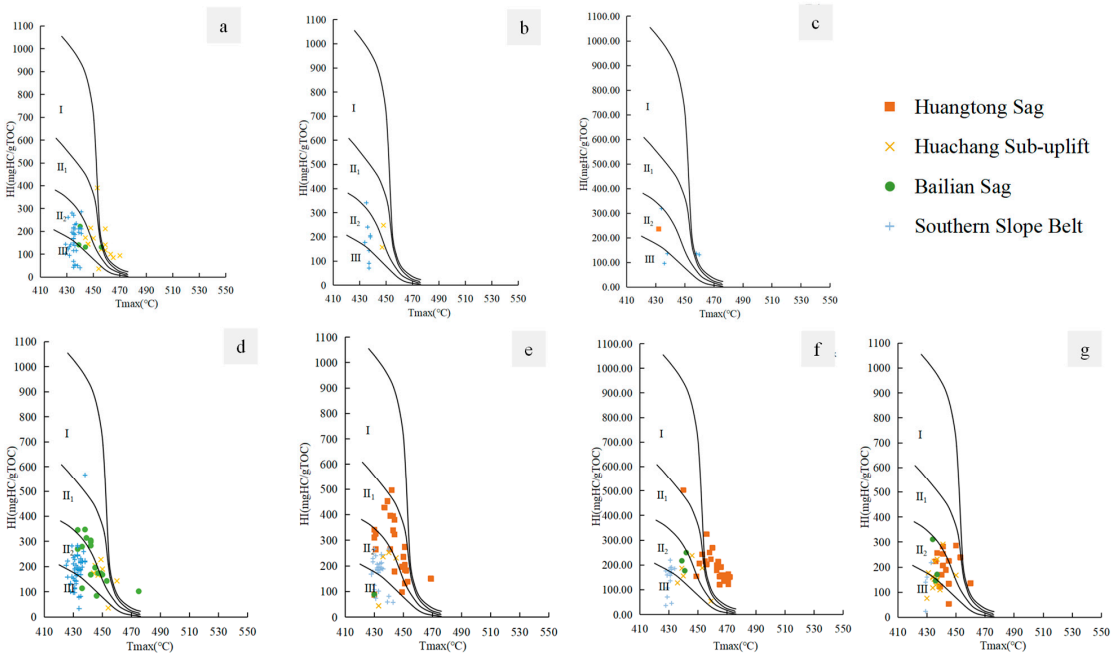

Figure 7. The relationship between HI and Tmax of source rocks in the Huangtong sag, Huachang Sub-uplift, Bailian Sag, and Southern Slope Belt in the Fushan Depression. The predominant type of organic matter is classified as type II_2. (**a**) E_2L_{3X} source rocks; (**b**) E_2L_{3Z} source rocks; (**c**) E_2L_{3S} source rocks; (**d**) E_2L_{2X} source rocks; (**e**) E_2L_{2S} source rocks (**f**) E_2L_{1X} source rocks; and (**g**) E_2L_{1S} source rocks. Thermal maturity of organic matter (after [24]).

The distribution range of E_2L_3 types II_2 and III organic matter is the widest, and the type of E_2L_{3S} organic matter is better with mainly type II_1. The E_2L_2 organic matter type is better in the Huangtong Sag and Huachang Sub-uplift, mainly type II_1. The organic matter type of E_2L_1 is better in the Huangtong Sag and Huachang Sub-uplift, mainly type II_2, and type II_1 exist. The type II_2 organic matter of E_2L_1 has the widest distribution area.

The hydrocarbon generation threshold for the Huangtong Sag, Bailian Sag, and Huachang Sub-uplift is delineated by the depth at which the vitrinite reflectance of source rocks reaches a value of 0.5%, which corresponds to a threshold depth of approximately 2800 meters. Consequently, the majority of the E_2L_1 source rocks have reached the threshold for hydrocarbon generation. The source rocks have also reached the peak of oil generation, and the depth above 4200 m has entered the high maturity stage. The E_2L_2 source rock is in the low maturity stage of development in the Huachang Sub-uplift. The E_2L_{2X} and E_2L_3 source rocks have reached the peak of oil generation and have entered the high maturity stage at a depth of 4200 m. The burial depth of the Southern Slope Belt is shallow, so the maturity of the source rock is also low. The variation trend in the vitrinite reflectance of the Southern Slope Belt source rocks with depth, shows that the threshold depth corresponding to the hydrocarbon generation threshold (Ro = 0.5%) is 2550 m and 1900 m, respectively (Tables 2 and 3, Figure 8).

Table 2. Rock-Eval pyrolysis data used in this study.

Area	Well	Depth	Formation	Sapropelic	Liptinite	Vitrinite	Inertinite	Type Coefficient	Organic Matter Type	Ro (%)	N	Std. Dev.
Huangtong Sag	C6X	2408.42	E_2L_{1S}	61.3	-	38.7	-	32.3	II_2	-	-	-
Huangtong Sag	C6X	2683.85	E_2L_{1S}	63.7	-	36.3	-	36.5	II_2	-	-	-
Huangtong Sag	C6X	2685.97	E_2L_{1S}	74.3	-	25.7	-	55	II_1	-	-	-
Huachang Sub-uplift	H1	2250	E_2L_{1S}	20.3	1	76.3	2.3	-	II_1	0.44	35	0.0002
Huachang Sub-uplift	H1	2300	E_2L_{1S}	22.3	1.3	73.3	3	-	II_1	0.41	31	0.0001
Huachang Sub-uplift	H1	2400	E_2L_{1S}	23.3	2.3	70.7	3.7	-	II_1	0.44	26	0.0039

Table 2. *Cont.*

Area	Well	Depth	Formation	Sapropelic	Liptinite	Vitrinite	Inertinite	Type Coefficient	Organic Matter Type	Ro (%)	N	Std. Dev.
Huachang Sub-uplift	H131x	2983.62	E_2L_{1S}	-	75	19	6	17.3	II_2	0.84	30	0.08
Huachang Sub-uplift	H132a	3447.35	E_2L_{1S}	-	73	19	8	14.3	II_2	0.78	27	0.06
Huachang Sub-uplift	H132a	3448.62	E_2L_{1S}	-	72	23	5	13.8	II_2	0.73	30	0.06
Huachang Sub-uplift	H2-2	2141.45	E_2L_{1S}	74.7	5.7	19.7	-	62.8	II_1	-	-	-
Huachang Sub-uplift	H2-2	2145.41	E_2L_{1S}	73.7	4	22.3	-	59	II_1	-	-	-
Huachang Sub-uplift	H2-2	2149.4	E_2L_{1S}	53.7	5.7	40.7	-	26	II_2	-	-	-
Huachang Sub-uplift	H2-2	2150.1	E_2L_{1S}	48	6.7	45	0.3	17.3	II_2	-	-	-
Huachang Sub-uplift	H2-2	2159.5	E_2L_{1S}	53.3	1	45.7	-	19.5	II_2	-	-	-
Huachang Sub-uplift	H7	2401.62	E_2L_{1S}	-	73	18	9	14	II_2	0.57	30	0.03
Huangtong Sag	J1x	3214.39	E_2L_{1S}	-	77	19	4	20.3	II_2	0.74	30	0.06
Huangtong Sag	J2x	3560.3	E_2L_{1S}	-	72	24	4	14	II_2	0.72	24	0.06
Huangtong Sag	J2X	3561.97	E_2L_{1S}	-	75	22	3	18	II_2	0.71	30	0.05
Huangtong Sag	J2X	3563.5	E_2L_{1S}	-	69	27	4	10.3	II_2	0.73	23	0.05
Huangtong Sag	Y10X	3276.1	E_2L_{1S}	65.7	-	34.3	-	40	II_2	-	-	-
Huangtong Sag	Y11X	3289.29	E_2L_{1S}	54.3	-	45.3	0.3	20	II_2	-	-	-
Huangtong Sag	Y11X	3548.9	E_2L_{1S}	69.3	-	30.7	-	46.3	II_1	-	-	-
Huangtong Sag	Y11X	3550.95	E_2L_{1S}	67.7	0.3	32.0	-	43.9	II_1	-	-	-
Huangtong Sag	Y11X	3552.53	E_2L_{1S}	76.0	-	24.0	-	58	II_1	-	-	-
Huangtong Sag	Y11X	3555.93	E_2L_{1S}	71.3	-	28.7	-	49.8	II_1	-	-	-
Huangtong Sag	Y11X	3557.93	E_2L_{1S}	67.0	-	33.0	-	42.3	II_1	-	-	-
Huangtong Sag	Y11X	3567.72	E_2L_{1S}	66.3	-	33.7	-	41	II_1	-	-	-
Huangtong Sag	Y11X	3568.92	E_2L_{1S}	69.0	-	31.0	-	45.8	II_1	-	-	-
Huangtong Sag	Y11X	3641.8	E_2L_{1S}	66.0	-	34.0	-	40.5	II_1	-	-	-
Huangtong Sag	Y11X	3643.65	E_2L_{1S}	65.7	-	34.3	-	40	II_2	-	-	-
Huangtong Sag	Y11X	3647.45	E_2L_{1S}	68.7	-	31.3	-	45.2	II_1	-	-	-
Huangtong Sag	Y11X	3653.12	E_2L_{1S}	68.7	-	31.3	-	45.2	II_1	-	-	-
Huangtong Sag	Y13x	3586.7	E_2L_{1S}	-	69	24	7	9.5	II_2	0.8	30	0.06
Huangtong Sag	C6-2X	2939.5	E_2L_{1X}	78.0	-	22.0	-	61.5	II_1	-	-	-
Huangtong Sag	C6-2X	2943.5	E_2L_{1X}	65.0	-	35.0	-	38.8	II_2	-	-	-
Huachang Sub-uplift	H1	2500	E_2L_{1X}	40.7	2.7	54	2	-	III	0.534	0	0
Huachang Sub-uplift	H1	2600	E_2L_{1X}	33.7	3	61	2	-	III	0.45	23	0.0034
Huachang Sub-uplift	H123-8X	3526.64	E_2L_{1X}	44.0	-	56.0	-	2	II_2	-	-	-
Huangtong Sag	Y10X	3499.67	E_2L_{1X}	80.7	-	19.3	-	66.2	II_1	-	-	-
Huangtong Sag	Y10X	3540.29	E_2L_{1X}	72.0	0.3	27.7	-	51.4	II_1	-	-	-
Huangtong Sag	Y11X	3670.48	E_2L_{1X}	71.7	0.3	28.0	-	50.9	II_1	-	-	-
Huangtong Sag	Y11X	3683.95	E_2L_{1X}	69.3	-	30.7	-	46.3	II_1	1.05	22	0.0275
Huangtong Sag	Y11X	3691.65	E_2L_{1X}	69.7	0.3	30.0	-	47.4	II_1	-	-	-
Huangtong Sag	Y11X	3694.9	E_2L_{1X}	72.0	-	28.0	-	51	II_1	-	-	-
Huangtong Sag	Y11X	3708.33	E_2L_{1X}	71.0	-	29.0	-	49.3	II_1	-	-	-
Huangtong Sag	Y11X	3715.74	E_2L_{1X}	77.7	-	22.3	-	61	II_1	-	-	-
Huangtong Sag	Y11X	3721.71	E_2L_{1X}	70.3	-	29.7	-	48	II_1	-	-	-
Huangtong Sag	Y11X	3725.29	E_2L_{1X}	77.3	-	22.7	-	60.3	II_1	-	-	-
Huangtong Sag	Y11X	3732.24	E_2L_{1X}	73.7	0.3	26.0	-	54.4	II_1	-	-	-
Huangtong Sag	C12X	3473.47	E_2L_{2S}	72	-	28	-	51	II_1	-	-	-
Huangtong Sag	C12X	3475.87	E_2L_{2S}	69.7	-	30.3	-	47	II_1	-	-	-
Huangtong Sag	C12X	3511.8	E_2L_{2S}	68.7	-	31.3	-	45.2	II_1	-	-	-
Huangtong Sag	C12X	3513.55	E_2L_{2S}	74	-	26	-	54.5	II_1	-	-	-
Huangtong Sag	C20X	1399.19	E_2L_{2S}	64.3	0.3	35.3	-	62.5	II_2	-	-	-
Huangtong Sag	C20X	1399.19	E_2L_{2S}	70.3	-	29.7	-	38	II_1	-	-	-
Huangtong Sag	C20X	1399.19	E_2L_{2S}	72.3	0.3	27.3	-	48	II_1	-	-	-
Huangtong Sag	C20X	1399.19	E_2L_{2S}	75.3	0.7	24	-	52	II_1	-	-	-
Huangtong Sag	C20X	1399.19	E_2L_{2S}	78.3	0.3	21.3	-	57.6	II_1	-	-	-
Huangtong Sag	C6X	3160.25	E_2L_{2S}	76.3	-	23.7	-	58.5	II_1	-	-	-
Huachang Sub-uplift	H1	2700	E_2L_{2S}	77.3	3.3	18.7	0.7	64.2	II_1	0.44	35	0.001
Huachang Sub-uplift	H1	2800	E_2L_{2S}	57	9.7	32.7	0.7	36.6	II_2	0.45	8	0.0061
Huachang Sub-uplift	H1	2900	E_2L_{2S}	86.7	0.7	12.7	-	77.5	II_1	0.49	34	0.0001
Huangtong Sag	J1x	3606.05	E_2L_{2S}	-	72	23	5	13.8	II_2	0.6	28	0.05
Huangtong Sag	J1x	3620.45	E_2L_{2S}	-	80	15	5	23.8	II_2	0.67	30	0.06
Huangtong Sag	Y7	3744.12	E_2L_{2S}	-	69	26	5	10	II_2	0.87	30	0.07
Huangtong Sag	Y7	3889.94	E_2L_{2S}	-	69	25	6	9.8	II_2	1.01	24	0.06
Huachang Sub-uplift	H1	3000	E_2L_{2X}	61	1.7	36.7	0.7	33.6	II_2	0.51	39	0.0017
Huachang Sub-uplift	H1	3100	E_2L_{2X}	66	1.7	31	1	42.8	II_2	0.52	34	0.0007

Table 2. *Cont.*

Area	Well	Depth	Formation	Sapropelic	Liptinite	Vitrinite	Inertinite	Type Coefficient	Organic Matter Type	Ro (%)	N	Std. Dev.
Huachang Sub-uplift	HD1-1	3332.25	E_2L_{2X}	-	69	23	8	9.3	II_2	1.03	25	0.06
Huachang Sub-uplift	HD1-1	3341.8	E_2L_{2X}	-	77	16	7	19.5	II_2	0.96	30	0.06
Huachang Sub-uplift	H1	3151	E_2L_{3S}	76	4	19	1	62.8	II_1	0.67	26	0.1288
Huachang Sub-uplift	H1	3165	E_2L_{3S}	59.7	2.3	36.3	1.7	31.9	II_2	0.64	19	0.133
Huachang Sub-uplift	H1	3195	E_2L_{3S}	54.7	1.3	42	1.7	-	II_2	0.54	30	0.001
Huachang Sub-uplift	H1	3300	E_2L_{3S}	37.3	0.7	60	1.7	-	III	0.57	30	0.0001
Huachang Sub-uplift	H7	3410.81	E_2L_{3S}	-	70	22	8	10.5	II_2	0.62	27	0.05
Huachang Sub-uplift	H7	3448.67	E_2L_{3S}	-	70	20	10	10	II_2	0.86	30	0.06
Huachang Sub-uplift	HD6-1X	3673.13	E_2L_{3S}	81.3	1.0	17.3	0.3	68.5	II_1	-	-	-
Huachang Sub-uplift	HD6-1X	3678.08	E_2L_{3S}	78.7	0.7	20.3	0.3	63.5	II1	-	-	-
Huachang Sub-uplift	H1	3400	E_2L_{3Z}	81.7	0.3	17.3	0.7	-	II1	0.54	30	0.0032
Huachang Sub-uplift	H1	3500	E_2L_{3Z}	24	1.3	69.3	5	-	III	0.56	30	0.0014
Southern Slope Belt	M17x	3801.56	E_2L_{3Z}	-	72	20	8	13	II_2	0.99	30	0.06
Southern Slope Belt	M17x	3804.1	E_2L_{3Z}	-	74	19	7	15.8	II_2	0.97	26	0.06
Huachang Sub-uplift	H1	3600	E_2L_{3X}	58.3	1	37.7	3	-	II_2	-	-	-
Huachang Sub-uplift	H1	3700	E_2L_{3X}	70	1.3	27.7	1	-	II_1	0.9	0	0
Huachang Sub-uplift	H1	3795	E_2L_{3X}	61.3	2	35.7	1	-	II_2	0.55	37	0.0012

Table 3. Rock-Eval pyrolysis data used in the sample of the Liushagang Formation in the Fushan Depression.

Area	Well	Depth (m)	Formation	Mudstone Color	TOC (wt %)	Extracted Bitumen "A" (%)	Tmax (°C)	S_1(mg HC/g Rock)	S_2(mg HC/g Rock)	$S_1 + S_2$ (mg HC/g Rocks)	Ro (%)
Bailian Sag	L1	2749	E_2L_{2X}	grey black	1.85	0.20	475	0.72	1.99	2.71	0.51
Bailian Sag	L102X	3234	E_2L_{1X}	brown grey	0.78	0.04	441	0.06	1.40	1.46	0.68
Bailian Sag	L2	3133	E_2L_{2X}	grey black	0.94	0.07	450	0.13	1.63	1.76	0.66
Bailian Sag	L22X	2079	E_2L_{3S}	dark grey	1.10	0.07	439	0.27	1.61	1.88	0.51
Bailian Sag	L23-1	3570	E_2L_{1X}	grey black	1.42	0.08	436	0.37	3.12	3.49	0.63
Bailian Sag	L23-1	4062	E_2L_{2X}	grey black	2.02	0.15	439	0.70	2.70	3.4	0.99
Bailian Sag	L23-1	3975	E_2L_{2S}	grey black	1.65	0.13	437	0.60	2.44	3.04	0.92
Bailian Sag	L23-1	3860	E_2L_{2S}	grey black	1.24	0.02	423	0.23	0.60	0.83	0.87
Bailian Sag	L23x	3923.8	E_2L_{2X}	grey black	1.84	0.15	442	0.42	3.19	3.61	1.11
Bailian Sag	L23x	4047.42	E_2L_{2X}	brown grey	0.99	0.09	443	0.13	1.86	1.99	0.65
Bailian Sag	L23x	3928	E_2L_{2X}	grey black	1.29	0.07	458	0.25	0.84	1.09	1.49
Bailian Sag	L23x	3930.05	E_2L_{2X}	grey black	1.08	0.09	460	0.21	0.7	0.91	1.46
Bailian Sag	L23x	4033.06	E_2L_{2X}	brown grey	0.92	0.09	469	0.14	0.55	0.69	1.45
Bailian Sag	L23x	4035.26	E_2L_{2X}	brown grey	0.88	0.07	476	0.09	0.34	0.43	1.69
Bailian Sag	L27X	3531.8	E_2L_{2X}	dark grey	2.39	0.25	447	1.08	3.96	5.04	0.82
Bailian Sag	L27X	3524.36	E_2L_{2X}	dark grey	1.97	0.19	443	0.74	2.82	3.56	0.64
Bailian Sag	L27X	2936	E_2L_{2S}	dark grey	0.93	0.19	434	0.21	3.14	3.35	0.58
Bailian Sag	L27X	3594.35	E_2L_{2X}	dark grey	2.06	0.16	448	0.63	2.64	3.27	1.11
Bailian Sag	L27X	3601.07	E_2L_{2X}	dark grey	1.36	0.10	449	0.25	1.65	1.90	0.84
Bailian Sag	L27X	3604.55	E_2L_{2X}	dark grey	1.42	0.10	451	0.26	1.57	1.83	1.03
Bailian Sag	L3-2X	3429	E_2L_{2X}	brown grey	1.65	0.18	442	0.41	2.63	3.04	0.83
Huangtong Sag	C12X	3473.17	E_2L_{2S}	grey black	1.53	0.18	443	0.47	5.18	5.65	0.75
Huangtong Sag	C12X	3511.35	E_2L_{2S}	grey black	0.85	0.15	443	0.26	3.35	3.61	0.76
Huangtong Sag	C12X	3511.35	E_2L_{2S}	grey black	0.94	0.36	444	0.40	3.57	3.97	0.76
Huangtong Sag	C12X	3473.17	E_2L_{2S}	grey black	1.28	0.20	444	0.40	4.13	4.53	0.75
Huangtong Sag	C2	2493	E_2L_{2S}	grey	1.90	0.08	436	0.22	4.30	4.52	0.49
Huangtong Sag	C20X	1393.59	E_2L_{2S}	brown grey	1.33	0.06	430	0.08	4.13	4.21	0.39
Huangtong Sag	C20X	1393.59	E_2L_{2S}	brown grey	1.21	0.06	431	0.05	3.29	3.34	0.39

Table 3. *Cont.*

Area	Well	Depth (m)	Formation	Mudstone Color	TOC (wt %)	Extracted Bitumen "A" (%)	Tmax (°C)	S_1(mg HC/g Rock)	S_2(mg HC/g Rock)	$S_1 + S_2$ (mg HC/g Rocks)	Ro (%)
Huangtong Sag	C20X	1393.59	E_2L_{2S}	brown grey	1.07	0.04	430	0.06	3.65	3.71	0.39
Huangtong Sag	C20X	1393.59	E_2L_{2S}	brown grey	1.01	0.04	431	0.05	3.2	3.25	0.39
Huangtong Sag	C5X	3660	E_2L_{2S}	grey black	1.81	0.03	425	0.47	4.65	5.12	0.54
Huangtong Sag	C5X	3857	E_2L_{2S}	grey black	2.09	0.11	433	0.38	3.41	3.79	0.66
Huangtong Sag	C5X	3778	E_2L_{2S}	grey black	1.55	0.12	431	0.38	3.28	3.66	0.57
Huangtong Sag	C5X	3700	E_2L_{2S}	grey black	1.52	0.13	431	0.48	2.68	3.16	0.90
Huangtong Sag	C5X	3812	E_2L_{2S}	grey black	1.56	0.16	425	0.51	2.59	3.1	0.51
Huangtong Sag	Fc1	3129.97	E_2L_{1X}	grey black	3.61	0.14	433	0.46	6.29	6.75	0.64
Huangtong Sag	Fc1	3120.07	E_2L_{1X}	grey black	1.99	0.09	435	0.27	3.12	3.39	0.60
Huangtong Sag	Fc1	3371.37	E_2L_{2S}	grey black	1.51	0.10	437	0.30	2.82	3.12	0.55
Huachang Sub-uplift	H104X	2750	E_2L_{1S}	brown grey	1.13	0.05	437	0.05	1.59	1.64	0.52
Huachang Sub-uplift	H109-3X	2501	E_2L_{1S}	brown grey	1.01	0.11	434	0.15	1.65	1.80	0.50
Huachang Sub-uplift	H113X	3125	E_2L_{1S}	brown grey	2.04	0.26	435	0.30	3.27	3.57	0.54
Huachang Sub-uplift	H115X	2698	E_2L_{1X}	dark grey	1.04	0.54	400	2.96	3.29	6.25	0.57
Huachang Sub-uplift	H2-15X	2913	E_2L_{2S}	brown grey	1.86	0.20	440	0.91	4.92	5.83	0.67
Huachang Sub-uplift	H2-2	2145.8	E_2L_{1S}	brown grey	0.74	0.03	431	0.15	1.42	1.57	0.51
Huachang Sub-uplift	H2-2	2155.6	E_2L_{1S}	grey black	0.85	0.04	438	0.09	1.06	1.15	0.53
Huachang Sub-uplift	H2-2	2145.8	E_2L_{1S}	grey black	0.80	0.06	436	0.05	0.95	1.00	0.51
Huachang Sub-uplift	H2-2	2136.95	E_2L_{1S}	grey black	0.84	0.05	434	0.06	1.33	1.39	0.50
Huachang Sub-uplift	H2-2	2136.95	E_2L_{1S}	grey black	0.90	0.04	434	0.05	1.06	1.11	0.50
Huachang Sub-uplift	H3-13X	3471	E_2L_{3Z}	Black grey	1.89	0.15	447	0.48	3.22	3.7	0.83
Huachang Sub-uplift	H7-6X	3979	E_2L_{3S}	grey black	1.74	0.18	396	0.75	5.55	6.3	1.04
Huachang Sub-uplift	H7-6X	3199	E_2L_{2S}	brown grey	1.74	0.19	445	0.73	4.06	4.79	0.70
Huachang Sub-uplift	H7-6X	3097	E_2L_{1X}	brown grey	1.48	0.17	446	0.57	3.55	4.12	0.62
Huachang Sub-uplift	H7-7X	3899	E_2L_{3S}	grey black	2.30	0.34	395	1.24	4.65	5.89	0.83
Huachang Sub-uplift	H7-7X	3052	E_2L_{1X}	brown grey	1.57	0.17	439	0.43	2.91	3.34	0.66
Huachang Sub-uplift	H7-7X	2477	E_2L_{1S}	dark grey	0.62	0.06	430	0.07	0.45	0.52	0.56
Huachang Sub-uplift	HD4-3X	3370	E_2L_{2S}	Black grey	1.17	0.04	433	0.13	0.49	0.62	0.76
Huachang Sub-uplift	HD6-1X	3821	E_2L_{3S}	grey black	1.00	0.10	444	0.31	1.74	2.05	0.91
Bailian Sag	JF4X	1991	E_2L_{2X}	brown grey	1.14	0.19	436	0.50	5.76	6.26	0.41
Bailian Sag	JF6	2535	E_2L_{1X}	grey black	0.45	0.04	439	0.10	1.00	1.10	0.48
Huangtong Sag	Y1	3509	E_2L_{1X}	brown grey	1.47	0.06	449	0.17	2.27	2.44	0.82
Huangtong Sag	Y1	3200	E_2L_{1S}	grey black	0.84	0.06	445	0.08	1.89	1.97	0.63
Huangtong Sag	Y1	3801.4	E_2L_{1S}	grey black	0.97	0.08	469	0.13	1.45	1.58	1.03
Huangtong Sag	Y1	3040	E_2L_{1S}	grey black	0.52	0.06	441	0.11	1.31	1.42	0.70
Huangtong Sag	Y1	3650	E_2L_{1S}	brown grey	1.37	0.07	449	0.06	1.34	1.40	0.82
Huangtong Sag	Y1	2903	E_2L_{1S}	brown grey	0.94	0.05	445	0.04	1.26	1.30	0.66
Huangtong Sag	Y1	2990	E_2L_{1S}	grey black	0.53	0.01	445	0.04	0.29	0.33	0.77
Huangtong Sag	Y10X	3274.2	E_2L_{1X}	dark grey	1.09	0.09	458	0.25	2.73	2.98	0.84
Huangtong Sag	Y10X	3536.54	E_2L_{1X}	dark grey	1.27	0.11	451	0.17	2.6	2.77	0.99
Huangtong Sag	Y10X	3495.07	E_2L_{1X}	dark grey	1.28	0.10	463	0.27	2.29	2.56	0.95
Huangtong Sag	Y11X	3724.89	E_2L_{1X}	brown grey	1.05	0.03	469	0.17	1.56	1.73	1.07
Huangtong Sag	Y11X	3641.15	E_2L_{1X}	brown grey	0.90	0.07	465	0.28	1.38	1.66	1.05
Huangtong Sag	Y11X	3551.23	E_2L_{1X}	brown grey	1.86	0.06	460	0.19	5.01	5.20	0.95
Huangtong Sag	Y11X	3547.3	E_2L_{1X}	brown grey	1.16	0.11	456	0.18	2.35	2.53	0.87
Huangtong Sag	Y11X	3641.15	E_2L_{1X}	brown grey	1.86	0.07	469	0.33	2.98	3.31	1.05
Huangtong Sag	Y11X	3286.79	E_2L_{1S}	dark grey	1.01	0.09	450	0.32	2.89	3.21	0.80

Table 3. *Cont.*

Area	Well	Depth (m)	Formation	Mudstone Color	TOC (wt %)	Extracted Bitumen "A" (%)	Tmax (°C)	S_1 (mg HC/g Rock)	S_2 (mg HC/g Rock)	$S_1 + S_2$ (mg HC/g Rocks)	Ro (%)
Huangtong Sag	Y11X	3692.1	E_2L_{1X}	brown grey	1.27	0.03	471	0.12	1.56	1.68	1.05
Huangtong Sag	Y11X	3560.12	E_2L_{1X}	brown grey	1.25	0.07	466	0.23	2.40	2.63	1.04
Huangtong Sag	Y11X	3547.3	E_2L_{1X}	brown grey	1.08	0.13	464	0.41	2.31	2.72	0.87
Huangtong Sag	Y11X	3666.38	E_2L_{1X}	brown grey	1.19	0.13	466	0.21	1.90	2.11	1.06
Huangtong Sag	Y11X	3717.06	E_2L_{1X}	brown grey	1.00	0.06	471	0.20	1.31	1.51	1.09
Huangtong Sag	Y11X	3551.23	E_2L_{1X}	brown grey	1.98	0.32	459	0.44	4.42	4.86	0.95
Huangtong Sag	Y11X	3641.15	E_2L_{1X}	brown grey	1.03	0.20	467	0.23	1.65	1.88	1.05
Huangtong Sag	Y11X	3551.23	E_2L_{1X}	brown grey	0.78	0.26	456	0.78	2.53	3.31	0.95
Huangtong Sag	Y11X	3724.89	E_2L_{1X}	brown grey	0.90	0.03	468	0.17	1.21	1.38	1.07
Huangtong Sag	Y11X	3560.12	E_2L_{1X}	brown grey	1.14	0.07	463	0.25	2.28	2.53	1.04
Huangtong Sag	Y11X	3683.95	E_2L_{1X}	brown grey	1.10	0.09	471	0.21	1.79	2.00	1.05
Huangtong Sag	Y11X	3700.36	E_2L_{1X}	brown grey	1.25	0.05	465	0.15	1.51	1.66	1.08
Huangtong Sag	Y11X	3675.25	E_2L_{1X}	brown grey	1.14	0.06	472	0.15	1.73	1.88	1.08
Huangtong Sag	Y11X	3560.12	E_2L_{1X}	brown grey	1.34	0.10	463	0.34	2.61	2.95	1.04
Huangtong Sag	Y7	3779.5	E_2L_{2S}	dark grey	1.96	0.14	441	0.29	4.42	4.71	0.84
Huangtong Sag	Y7	3782.35	E_2L_{2S}	dark grey	1.78	0.13	442	0.34	3.73	4.07	0.82
Huangtong Sag	Y7	3777.4	E_2L_{2S}	dark grey	1.48	0.13	438	0.23	3.13	3.36	0.72
Huangtong Sag	Y7	3785.15	E_2L_{2S}	dark grey	1.35	0.12	441	0.26	3.06	3.32	0.79
Huangtong Sag	Y7	3742.1	E_2L_{2S}	grey black	1.41	0.08	440	0.16	3.06	3.22	0.69
Huangtong Sag	Y7	3892.3	E_2L_{2S}	dark grey	1.83	0.14	449	0.41	2.07	2.48	0.92

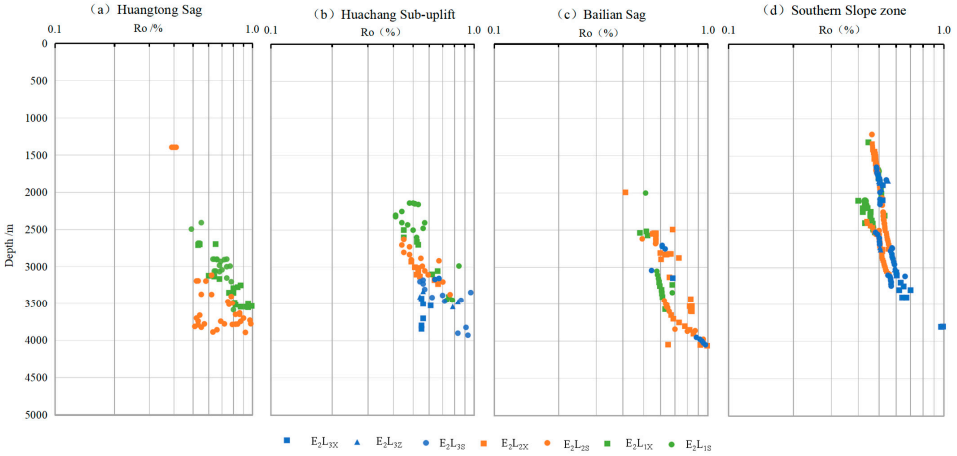

Figure 8. Variation in the vitrinite reflectance of source rocks of E_2L_{3X}, E_2L_{3Z}, E_2L_{3S}, E_2L_{2X}, E_2L_{2S}, E_2L_{1X}, and E_2L_{1S} sequentially with depth in the Fushan Depression. (**a**) Huangtong Sag, (**b**) Huachang Uplift, (**c**) Bailian Sag, and (**d**) Southern Slope Belt. The overall variation in the Rock-Eval pyrolysis parameter, *Ro*, exhibits a positive correlation with the increase in burial depth.

In summary, the Southern Slope Belt crossed the hydrocarbon generation threshold during the early phase of the E_2L_2 source rock but has not yet reached the zenith of oil generation. In general, the high-grade area of *Ro* in the Liushagang Formation is located in the Huangdong Sag and Bailian Sag, and the overall change is positively correlated with the increase in burial depth. From E_2L_{2X} to E_2L_3, the maturity in the east is significantly higher than in the other regions, which is related to the intrusion of igneous rocks in E_2L_2 and E_2L_3. The thermal effect makes it appear as an unusually high-maturity area, up to 2.69% ([7,75]) (Figure 9).

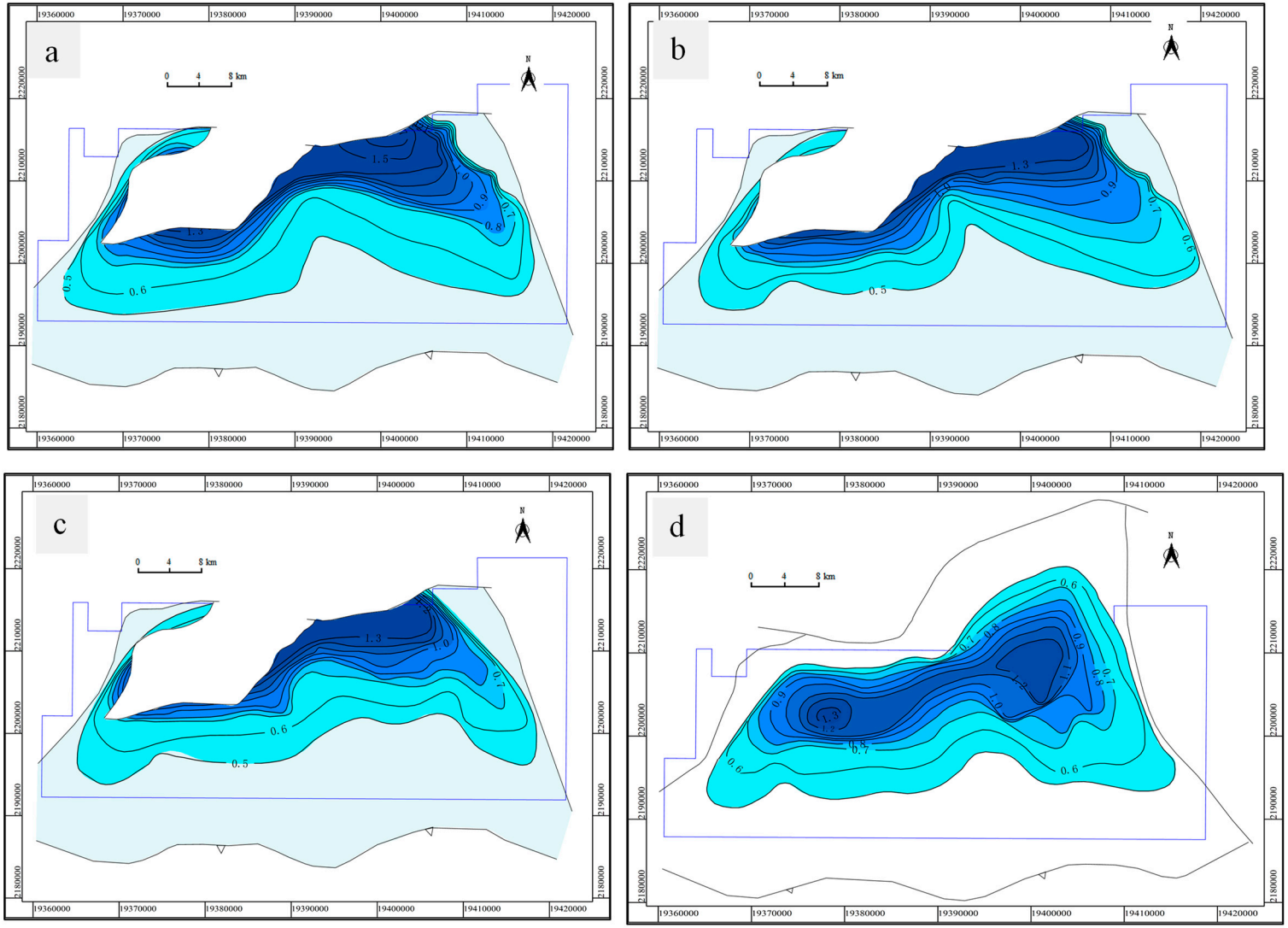

Figure 9. *Cont*.

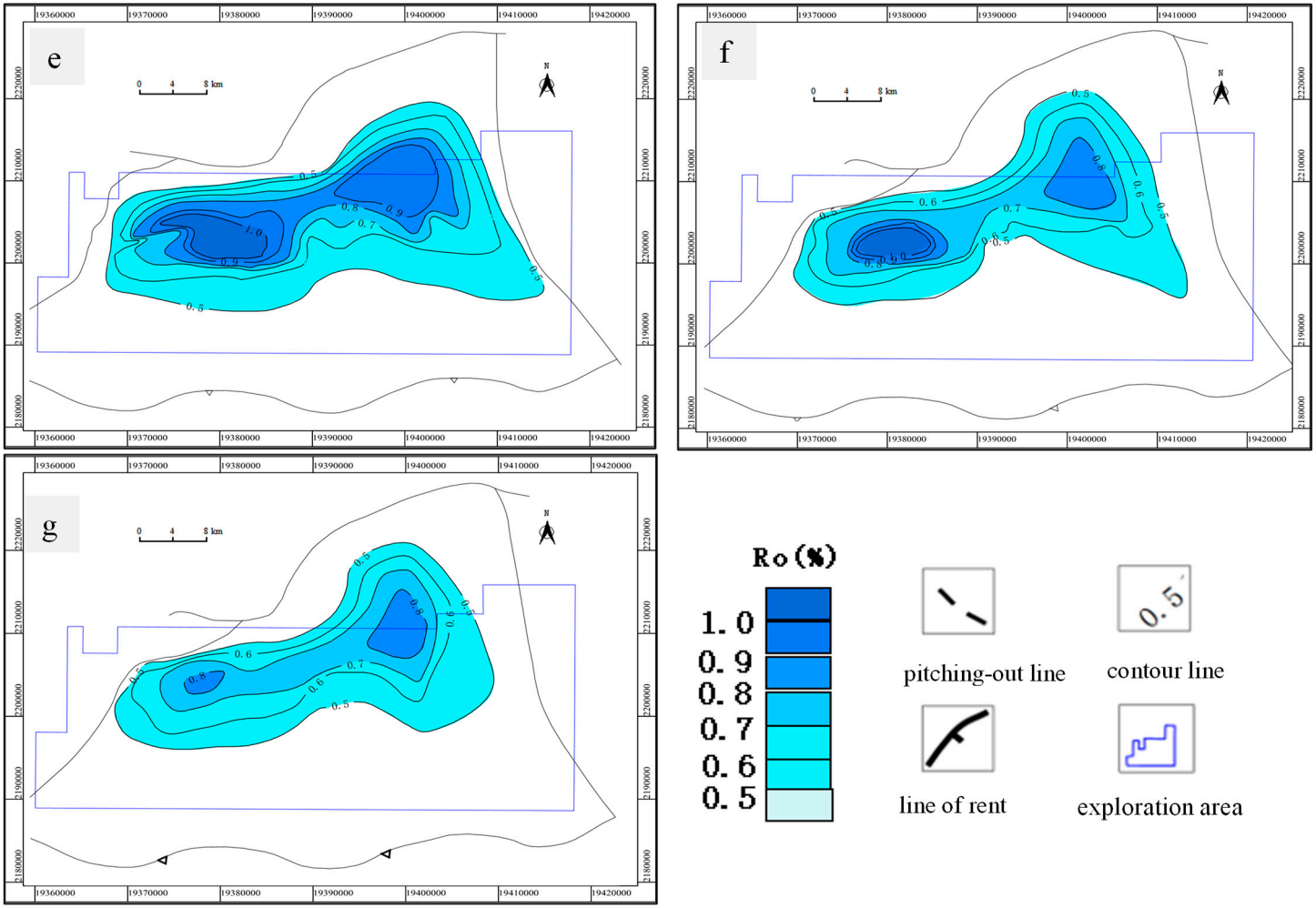

Figure 9. Ro plane contour map of source rocks in the Liushagang Formation in the Fushan Depression. The region of elevated Ro values is situated within the Huangtong Sag and the Bailian Sag. There is a gradual decrease in Ro values from these high-value areas towards the periphery of the respective depressions. (**a**) E_2L_{3X} source rocks; (**b**) E_2L_{3Z} source rocks; (**c**) E_2L_{3S} source rocks; (**d**) E_2L_{2X} source rocks; (**e**) E_2L_{2S} source rocks; (**f**) E_2L_{1X} source rocks; and (**g**) E_2L_{1S} source rocks.

5. Geological Characteristics of Source Rocks

The average thickness of the E_2L_3 source rock formation is less than 100 m, demonstrating a progressive reduction in thickness from the vicinity of the Meihua Fault towards the Southern Slope Belt. The E_2L_{3X} source rock, proximal to the Meihua Fault control boundary, is estimated to attain a maximum thickness of approximately 295 m. Within the Huangtong Sag and Bailian Sag, the E_2L_2 source rocks exhibit an average thickness exceeding 400 m, with a lateral extent that transitions from the central regions of the sags towards their peripheries. Within the central region of the Huachang Sub-uplift, a significant elevation of 424 m is observed, comparable to the other two sags. The E_2L_1 source rock in the Huangtong Sag, Bailian Sag, and Huachang Sub-uplift exhibits a similar thickness, reaching a maximum of 531 m. The significant thickness of the source rock is predominantly observed in the Huangtong and Bailian Sags, exhibiting a gradual reduction towards their peripheries (Figure 4). The E_2L_{2X} dark mudstone is exceptionally well-developed. In comparison with the source rocks from other stratigraphic units, the E_2L_{2S} source rock exhibits a substantial thickness of 750 m. Furthermore, the E_2L_{2S} source rock, with a thickness exceeding 250 m, is characterized by a more extensive areal distribution.

The stratigraphic thickness of the dark mudstone serves as a pivotal determinant in ascertaining the thickness of the effective source rocks [61]. The areal extent and stratigraphic thickness of E_2L_3, characterized by dark mudstone, are significantly less extensive than those of E_2L_1 and E_2L_2. The northern strata of the E_2L_3 formation have been eroded along the fault line. During the depositional phases of the E_2L_{3X} and E_2L_{3Z} members, a singular subsidence center was established in the northeastern part of the Bailian Sag, where the sedimentary thickness is predominantly concentrated. This could be attributed to the influence of the Meihua Fault, with source supply from the northwest and southwest directions [54]. Within E_2L_{3S}, the Huangtong and Bailian Sags are characterized as two principal subsidence centers. Initially, during the depositional phase of the E_2L_{2X} formation, the expanse of dark mudstone in the deep-depression zone, specifically in the northern sector adjacent to the Meihua Fault, exhibited a more extensive distribution. At present, the subsidence center remains constant. Because of the relatively deep and stable hydrosphere, there is extensive development of thick dark mudstone within the reducing environment. For example, the thickness of the dark mudstone in the H18X well is 360 m, which is 100% of the thickness of the E_2L_{2X} formation, and the whole section is dark mudstone. Affected by the southern provenance [61], the distribution range of E_2L_{2S} in the Huangtong Sag becomes smaller; however, the dark mudstone of fan delta plain facies with a thickness of 570 m is developed in the C4X well. The thickness of source rock in the Huachang Sub-uplift is high, and the thickness of the E_2L_{2S} source rock is larger than that of the other layers. Under the condition that the subsidence center of E_2L_{1X} is unchanged, the thickness of the source rock in the deep depression area is smaller than that in E_2L_2. The hydrocarbon charge to the Huachang Sub-uplift, located in the southern sector of the E_2L_{1S}, has experienced a reduction in source input, resulting in the re-establishment of two subsidence centers, while concurrently, the areal extent of the source rock has diminished. Overall, the source rocks of the Liushagang Formation are mainly distributed in Sags, and the thickness and area of E_2L_2 source rocks are the largest (Figure 10).

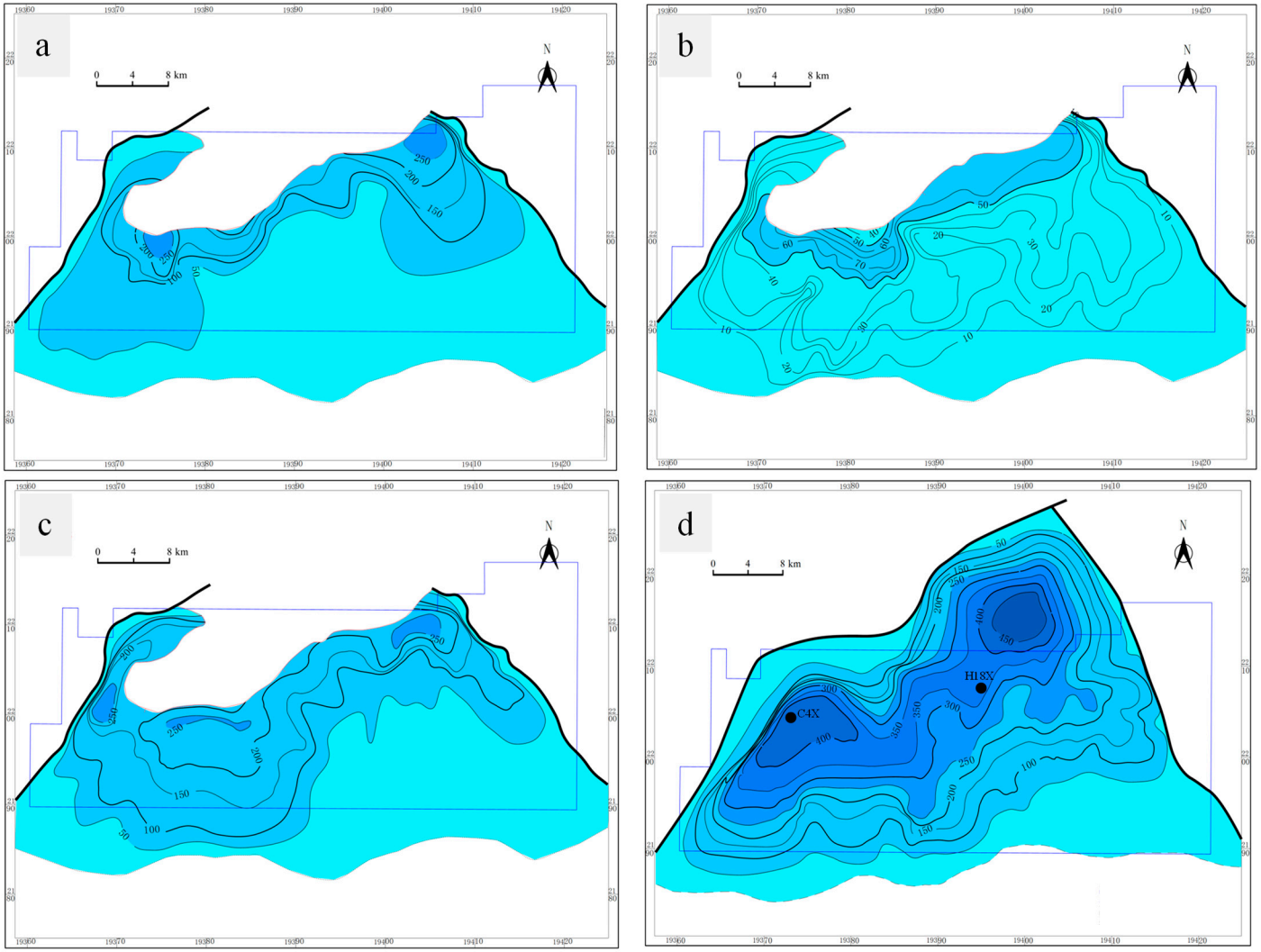

Figure 10. *Cont*.

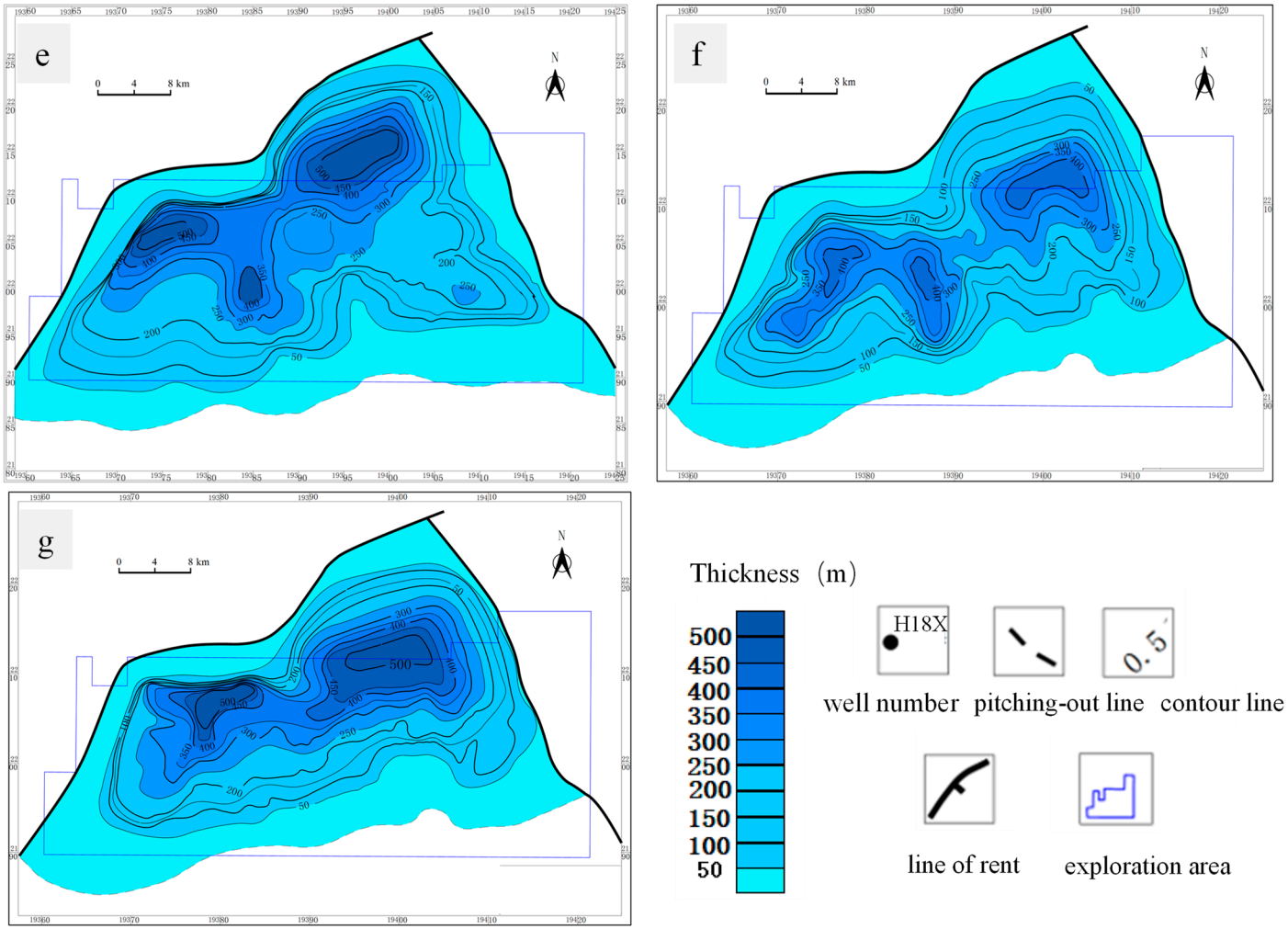

Figure 10. Source rock thickness contour map of the Liushagang Formation in the Fushan Depression. Influenced by the Meihua Fault, the provenance rocks of the Early Liushagang Formation in the northern region underwent significant denudation. The depositional center and the area of maximum thickness of these source rocks are observed in the Huangtong Sag and the Bailian Sag, respectively. (**a**) E_2L_{3X} source rocks; (**b**) E_2L_{3Z} source rocks; (**c**) E_2L_{3S} source rocks; (**d**) E_2L_{2X} source rocks; (**e**) E_2L_{2S} source rocks; (**f**) E_2L_{1X} source rocks; and (**g**) E_2L_{1S} source rocks.

6. Organic Petrology of Source Rocks

From the scatter data in the triangle diagram, it can be seen that the content of the sapropelic group and liptinite macerals of the E_2L_2 source rock is higher compared with the adjacent E_2L_1 and E_2L_3 sections, ranging from 62.7% to 87.4%, with an average of 72.57%. The sapropelic group is dominated by sapropelic amorphous bodies, and the content can reach more than 60%. The average vitrinite content is 25.56%, and the average inertinite content is 1.86%. The hydrocarbon-generating capacity of the organic matter in the E_2L_2 source rocks is high. In E_2L_{2S}, the content of the sapropelic group in the Huangtong Sag is higher, and there is no inertinite. The content ranges from 0.1% to 6.0%, with an average of 1.32%.

From the scatter data in the diagram (Table 2), it can be seen that the content of the E_2L_{2X} and E_2L_{2S} sapropel group and liptinite group is higher than that of the adjacent E_2L_1 and layers (Table 2, Figure 11). By calculating the maceral type index, it is concluded that type II_1 (40< *TI* <80) and type II_2 (0 < *TI* < 40) are the main organic matter types of the Liushagang Formation source rocks, and type I (80 < *TI*) and type III (*TI* < 0) kerogen are rarely developed, among which type II_1 kerogen accounts for 65% of all the samples. It can be concluded that dark mudstone has high organic matter content and hydrocarbon generation potential, and belongs to oil source rocks, especially those of the Huangtong Sag and Bailian Sag.

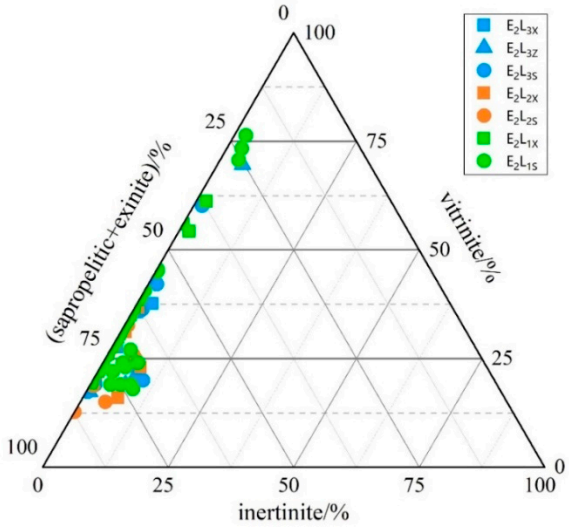

Figure 11. Triangle diagram of macerals of organic matter in the source rocks of the Liushagang Formation in the Fushan Depression. The sapropelic and exinitic maceral groups exhibit elevated concentrations, with values ranging from 62.7% to 87.4% and an average of 72.57%. As the principal constituents responsible for hydrocarbon generation, this high content underscores the robust hydrocarbon-generating potential of the organic matter.

Combined with the analysis of the two methods, the E_2L_{2X}, E_2L_{2S}, and E_2L_{1X} of the Huangtong Sag to the west are dominated by type II_1 kerogen, which develops mainly from deep lake mudstone, and the provenance is mainly from the south [76]. The type II_2 kerogen sample (well Y11X) of E_2L_{1S} in the Huangtong Sag has a sapropelic content of 54.3%, which is much lower than that of the other beds. During this period, the western source was supplied in large quantities [77]. The gravel at the base of E_2L_{1S} (2535.0 m) can be observed, and the sorting is 3.03. E_2L_{1S} has a high TOC (2.29%) at this time but has no hydrocarbon generation potential. The Bailian Sag in the eastern part of the survey area is dominated by type II_2 kerogen, but most of the wells in the Sag changed from type II_2 to type III at E_2L_{2X}. At this time, the eastern source supply was sufficient, the grain size increased to 22.4 mm, the deep lake mudstone was intercalated with turbidite sandstone, and the vitrinite content reached 36.7%. During the deposition of the Liushagang Formation in the Southern Slope Belt, there was a sufficient source from the south [78], mainly type

II_2 and type III kerogen. No sapropel group was identified in the M17 well observation, with 72% of the liptinite group. Affected by the source of the western source in the E_2L_{1X} period [7], tear-like mud particles appeared, the whole was inverted grain order, and there were multiple positive cycles.

This shows that the source supply is sufficient, the particle size increases, and the screening deteriorates. Meanwhile, the sapropel group content decreases, and the total HI decreases. This shows that during the depositional process of the Liushagang Formation, the external transport was mainly oxidized or polymerized vitrinite and inertinite, which have no hydrocarbon-generating capacity. At this time, the layer has high TOC but no hydrocarbon generation capacity. As the source supply weakens, the algae and debris in the lake basin produce sapropel, which has a high H index and hydrocarbon generation potential (Table 3, Figures 11 and 12).

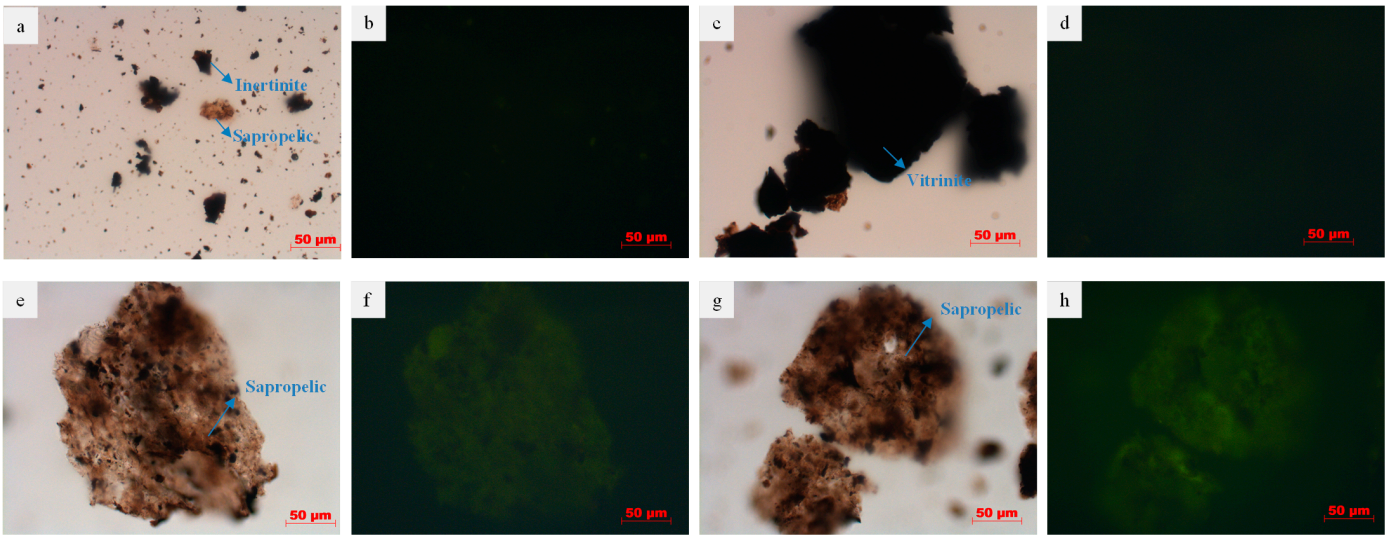

Figure 12. Microscopic identification of kerogen macerals and types of the Liushagang Formation in the Fushan Depression. (**a**) Y13X in the Huangtong Sag, E_2L_1, 3586.7 m, type III kerogen. The inertinite macerals can be observed, and (**b**) the sapropel group is not strongly reflected under fluorescence. (**c**) H7X in the Huachang Sub-uplift, E_2L_1, 2401.62 m, type III kerogen. (**d**) The vitrinite macerals can be observed. (**e**) Y7X in the Huangtong Sag, E_2L_1, 3744.12 m, type II_2 kerogen; (**f**) Development of sapropelic macerals. (**g**) H7X in the Huachang Sub-uplift, 3448.67 m, E_2L_3, type II_2 kerogen. (**h**) Compared with E_2L_1, more sapropelic macerals were developed.

7. Hydrocarbon Expulsion Characteristics of Source Rocks

7.1. Simulation of Hydrocarbon Generation and Expulsion History

The comprehensive analysis of the burial, thermal, and hydrocarbon generation histories for individual wells across the Fushan Depression reveals a consistent evolutionary pattern in hydrocarbon generation and expulsion within the source rock strata, albeit with minor temporal variations. The initial phase of hydrocarbon expulsion was observed in the deep depressions of the Huangtong Sag and Bailian Sag, succeeded by the Huachang Sub-uplift, and culminated in the Southern Slope Belt.

The Yong 7X well, located in the western sector of the study area, demonstrates evidence of burial following the sedimentation of the E_2L_2 formation. It experienced three transient uplift and denudation events at 42–41 Ma, 36–33 Ma, and 23.5–20 Ma, separately, before entering a phase of rapid burial. Hydrocarbon generation in the Yong 7 well began around 37 Ma, stabilizing at 25 Ma. E_2L_{2S} source rocks also initiated hydrocarbon generation around 37 Ma, with a significant increase in the generation rate compared with the lower sub-member of Liu II, reaching the expulsion threshold around 28 Ma and commencing hydrocarbon expulsion. Tectonic events, such as the Zhuqiong movement of the Hainan Uplift at 36 Ma and 23.5 Ma, temporarily weakened or halted hydrocarbon

generation and expulsion. The process resumed after further burial, with the restart time in the Huangtong Sag at 33 Ma and 20 Ma, respectively.

The burial and hydrocarbon generation history of the Lian 23 well in the Bailian Sag mirrors that of the Huangtong Sag, characterized by burial, three short uplift and denudation phases, and then followed by rapid burial. The hydrocarbon generation in the Lian 23 well during the E_2L_{2X} sedimentation period commenced around 36.5 Ma. E_2L_{2S} source rocks began generating hydrocarbons at a similar time but at a significantly higher rate than E_2L_{2X}. E_2L_2 reached the hydrocarbon expulsion threshold at approximately 24 Ma and 12 Ma, initiating expulsion. Similar to the Huangtong Sag, tectonic movements at 36 Ma and 23.5 Ma disrupted hydrocarbon generation and expulsion, which resumed after further burial, with restart times in the Bailian Sag at 33 Ma and 20 Ma (Figure 13).

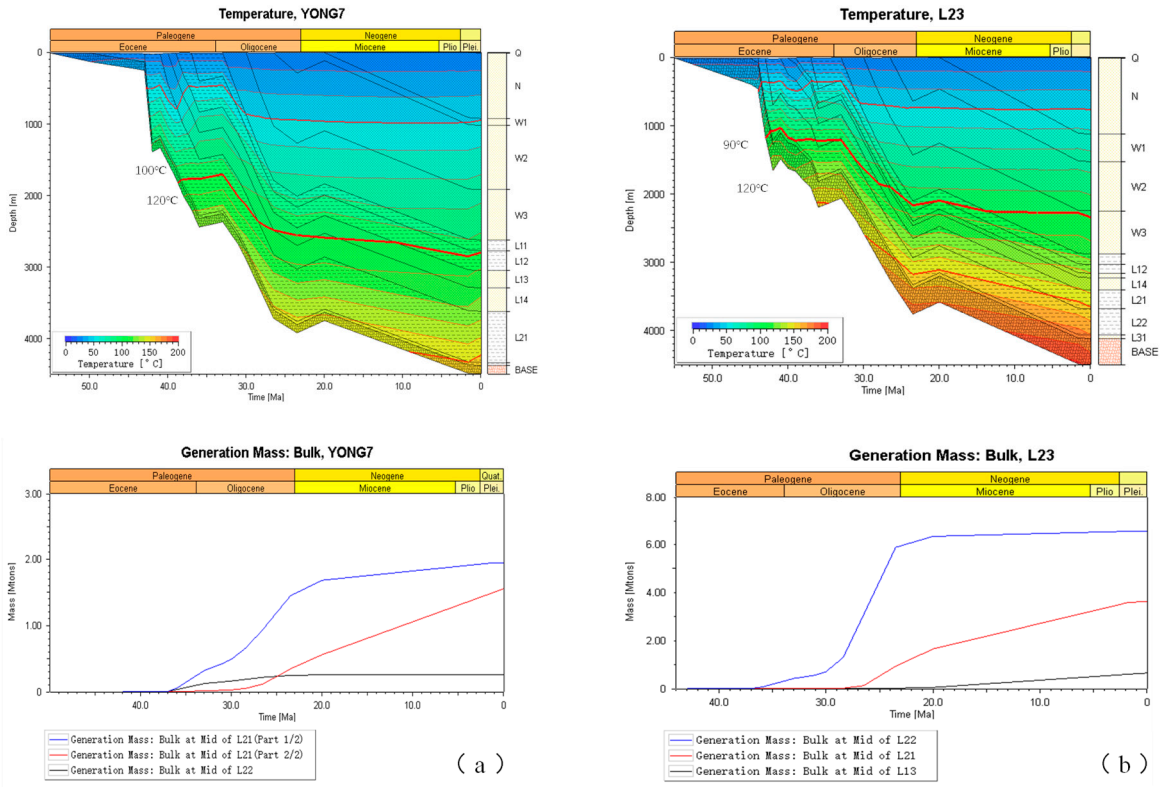

Figure 13. Sedimentary burial history and hydrocarbon generation history. (**a**) The Y7 well in the Huangtong Sag; (**b**) the L23 well in the Bailian Sag. The Huangtong Sag and the Bailian Sag predominantly accumulated hydrocarbons during the E_2L_2 and E_2L_1 epochs following the generation of hydrocarbons, indicative of an early phase of two-stage accumulation. Subsequently, the hydrocarbons migrated to the structural high areas, namely, the Huachang Sub-uplift and the Southern Slope Belt, marking a later phase characterized by one-stage accumulation.

These observations elucidate the impact of tectonic activities on the hydrocarbon generation and expulsion processes in the Fushan Depression, providing a refined understanding of the temporal evolution of hydrocarbon systems in this region.

7.2. Hydrocarbon Generation and Expulsion Models of Source Rocks

In accordance with the hydrocarbon generation and expulsion paradigm for the Fushan Depression, the source rocks are anticipated to cross the threshold for hydrocarbon generation at a depth of 2200 m and the threshold for hydrocarbon expulsion at 2700 m. The rates of hydrocarbon generation and expulsion initially increase and then decrease. Early in hydrocarbon generation, the rate changes little and remains low until reaching a peak generation rate at 2370 m, with a maximum value of 510 mg/g. After passing the expulsion threshold, hydrocarbon is gradually expelled as thermal evolution progresses,

with the expulsion rate peaking at 3220 m and a maximum value of 430 mg/g HC/g rock. Throughout the process, hydrocarbon expulsion efficiency increases, reaching a maximum of 88%.

Hydrocarbon displacement models for the three sets of source rocks (E_2L_1, E_2L_2, E_2L_3) in the Fushan Depression were also established. The hydrocarbon generation thresholds are 2200 m, 1850 m, and 2200 m, respectively, while the hydrocarbon expulsion thresholds are 2650 m, 2720 m, and 2640 m, respectively. The hydrocarbon expulsion peaks for these source rocks correspond to the burial depths of 3170 m, 3380 m, and 3600 m, respectively, with expulsion efficiencies exceeding 84%, indicating sufficient hydrocarbon expulsion. Differences in hydrocarbon expulsion characteristics among the Liushagang Formation source rocks are attributed to variations in burial history, thermal history, and the type and abundance of organic matter in different sedimentary intervals (Figure 14).

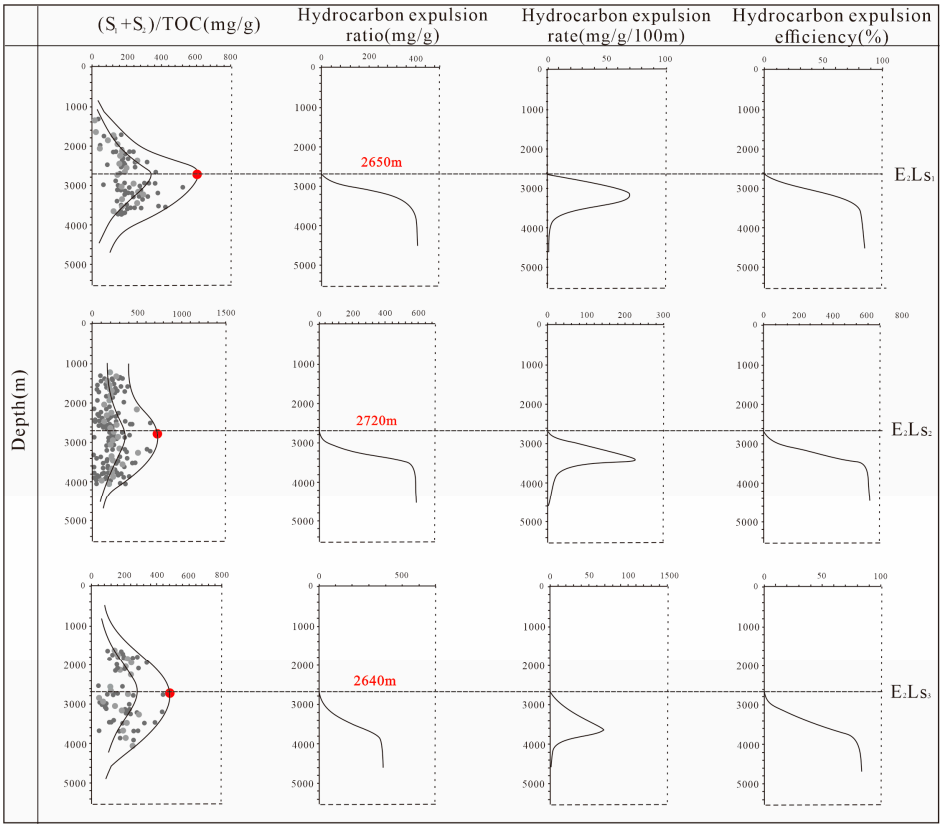

Figure 14. Hydrocarbon expulsion model of the Liushagang Formation in the Fushan Depression, the red spot is the hydrocarbon expulsion threshold to restore the maximum hydrocarbon generation potential index. Upon reaching the critical depths where the source rock crosses the thresholds for hydrocarbon generation and expulsion, the rate of hydrocarbon generation peaks at a depth of 2370 m. Conversely, at a depth of 3220 m, the expulsion rate of hydrocarbons is maximized, achieving a peak expulsion efficiency of 88%.

7.3. Hydrocarbon Generation, Expulsion Intensity, and Volume of Source Rocks

This study shows that there are some differences in the hydrocarbon expulsion period of the source rocks in each section of the Fushan Depression. Among them, the source rocks of E_2L_2 started to expel hydrocarbon in the Oligocene (the Huangtong Sag is 28 Ma; the Bailian Sag is 29 Ma). The source rocks of E_2L_3 started to expel hydrocarbons 26 Ma ago. The hydrocarbon source rocks of E_2L_1 started to produce hydrocarbons 25 Ma ago and migrated into the reservoir of the first member of the Liushagang Formation. This shows that from the beginning of the Oligocene, the source rocks of each layer began to expel a large amount of hydrocarbon, and the source rock hydrocarbon expulsion center of

E_2L_2 of the flow was the largest, reaching the peak period of the source rock hydrocarbon expulsion. The burial depth of the source rock at this time is consistent with the burial depth of the peak period of hydrocarbon expulsion of the TH.

7.4. Tight Oil Resource Potentials of Source Rocks

The centers of hydrocarbon generation and expulsion within the dark mudstone strata of the E_2L_1 and E_2L_2 formations are predominantly localized in the Huangtong Depression and the Bailian Depression. The maximum hydrocarbon generation intensity of E_2L_1 is 475 × 10^4 t/km^2 and 625 × 10^4 t/km^2, respectively, and the maximum hydrocarbon expulsion intensity is 185 × 104 t/km^2 and 230 × 10^4 t/km^2, respectively. Although the distribution areas of hydrocarbon generation and expulsion in the two layers are roughly similar, better than E_2L_1 in terms of the intensity, and it is a hydrocarbon generation stove with larger resources.

The hydrocarbon generation and expulsion epicenters within the E_2L_3 source rocks are predominantly localized in the Bailian Sag, Huangtong Sag, and Huachang Sub-uplift areas. Compared with E_2L_1 and E_2L_2, the main source rock of E_2L_3 in the Huachang Sub-uplift is added. The maximum hydrocarbon generation intensity is 240 × 10^4 t/km^2, and the maximum hydrocarbon expulsion intensity is 90 × 10^4 t/km^2.

In general, compared with the source rocks of the other two horizons, the hydrocarbon expulsion range of E_2L_2 is larger, and the hydrocarbon generation and expulsion intensities of the Bailian Sag are significantly higher than those of the Huangtong Sag (Figure 15).

The total volume of hydrocarbon generation and expulsion from the source rocks within the Fushan Sag were determined through the application of mathematical integration techniques, taking into account the spatial extent of the source rock formations and their respective intensities of hydrocarbon generation and expulsion. The total cumulative hydrocarbon generation amount in the Fushan Depression is 134.10 × 10^8 t, the cumulative hydrocarbon expulsion amount is 50.52 × 10^8 t, and the residual hydrocarbon amount is 83.58 × 10^8 t (Figure 16). In comparison to the source rocks of the other two stratigraphic horizons, the hydrocarbon expulsion window of the E_2L_2 formation is markedly broader. Moreover, the intensity of hydrocarbon generation and expulsion within the Bailian Sag is considerably more pronounced than that observed in the Huangtong Sag.

Overall, the hydrocarbon generation of the dark mudstone in E_2L_2 is 73.90 × 10^8 t, which is higher than that of other layers, accounting for 55.11% of the total hydrocarbon generation of the source rocks in the Liushagang Formation, followed by the source rocks in E_2L_1, accounting for 29.85%. The hydrocarbon generation in E_2L_3 is the least, accounting for 15.04%. The hydrocarbon seepage is similar. The source rock of the second member of the Liushagang Formation accounts for the highest proportion of 52.75%, and the hydrocarbon expulsion amount of the source rock of E_2L_1 and E_2L_3 account for only 32.03% and 15.22%, respectively. This shows that the main source rocks in the Fushan Depression are mainly dark mudstone in E_2L_2, while the contribution of source rocks in E_2L_1 and E_2L_3 is relatively small (Table 4).

Table 4. Data table of hydrocarbon generation and expulsion amount of source rocks in each layer of the Fushan Depression.

Formation	Hydrocarbon-Generating Quantity 10^8 t	The Proportion of Hydrocarbon Generation%	Hydrocarbon Expulsion Quantity 10^8 t	Proportion of Hydrocarbon Expulsion Amount %
E_2L_1	40.03	29.85	16.18	32.03
E_2L_2	73.90	55.11	26.65	52.75
E_2L_3	20.17	15.04	7.69	15.22
Total	134.10	100.00	50.52	100.00

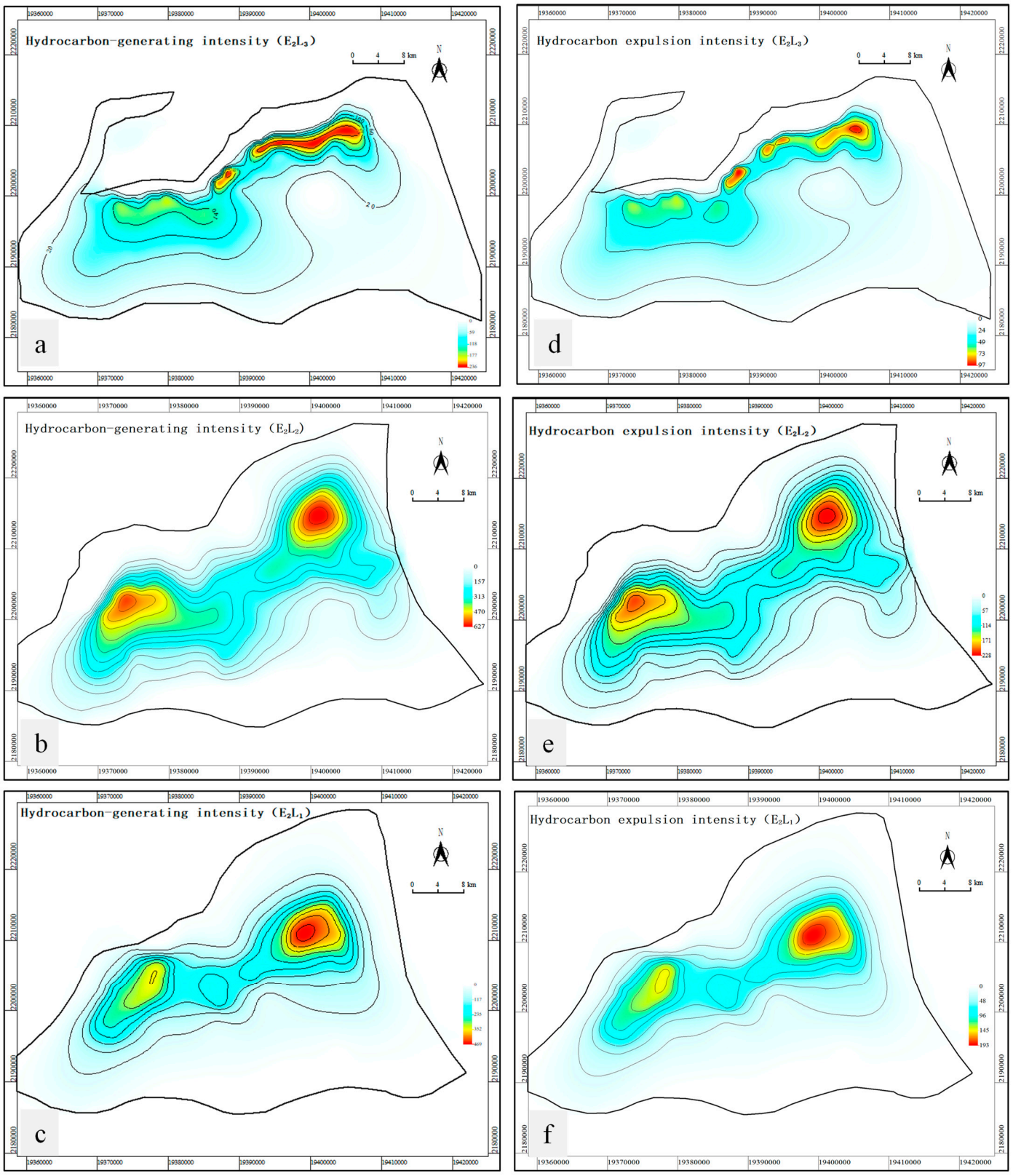

Figure 15. Contour map of hydrocarbon generation and expulsion intensity of source rocks in each layer of the Liushagang Formation in the Fushan Depression. (**a**) E_2L_3 source rocks; (**b**) E_2L_2 source rocks; (**c**) E_2L_1 source rocks; (**d**) E_2L_3 source rocks; (**e**) E_2L_2 source rocks; and (**f**) E_2L_1 source rocks.

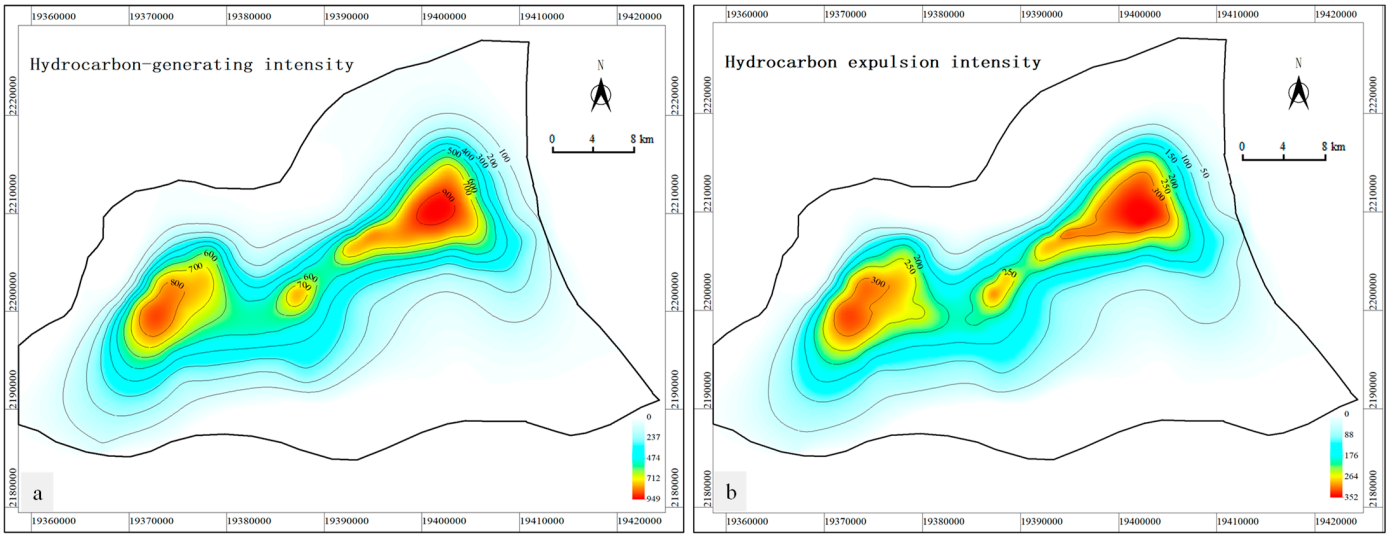

Figure 16. (**a**) Isoline diagram of hydrocarbon generation of the source rocks in the Liushagang Formation in the Fushan Depression. (**b**) Isoline diagram of expulsion intensity of the source rocks in the Liushagang Formation in the Fushan Depression. The E_2L_2 dark mudstone exhibits a higher hydrocarbon generation potential compared with the other strata. It shares similar characteristics in hydrocarbon expulsion and generation processes. In contrast, the contributions from the E_2L_3 and E_2L_1 source rocks are comparatively minor.

In light of the hydrocarbon expulsion calculations, and in conjunction with the geological framework of the sag, as well as integrating prior research findings, the accumulation coefficients for the source rocks across various strata within the Fushan Depression were ascertained as follows: 56% for E_2L_2, 25% for E_2L_1, and 10.5% for E_2L_3. The prospective resources of the source rocks in the Liushagang Formation of the Fushan Depression were calculated accordingly (Table 5). The prospective resources of E_2L_2 in the Fushan Depression are 14.92 $\times$ 10^8 tons, accounting for 75.46% of the total prospective resources. The dark mudstone resources of E_2L_1 and E_2L_3 account for 20.46% and 4.08%, respectively. Thus, the main source rocks in the Fushan Depression are the dark mudstone of E_2L_2. While E_2L_1 and E_2L_3 have some hydrocarbon potential and prospective resources, their contributions are relatively minor.

Table 5. Hydrocarbon source rock prospective resource data table for the Fushan Depression.

Formation	Hydrocarbon Expulsion Quantity 10^8 t	Migration and Accumulation Coefficient %	Predicted Resources 10^8 t	Proportion of Resources %
E_2L_1	16.18	25.00	4.05	20.46
E_2L_2	26.65	56.00	14.92	75.46
E_2L_3	7.69	10.00	0.81	4.08
Total	50.52	/	19.77	100.00

8. Conclusions

The maximum thickness of the source rock is observed in the subsidence centers of the Huangtong Sag (west) and the Bailian Sag (east), with a progressive thinning towards the periphery and the Huachang Sub-uplift. Dark mudstone predominantly occurs at depths below 200 m. The Liushagang Formation source rocks in the Fushan Depression show high organic matter abundance, particularly in the northern Huangtong Sag and the Bailian Sag. The average TOC is 1.80%, extractable bitumen 'A' is 0.1279%, and the hydrocarbon generation potential (S_1 + S_2) is 3.63 mg/g. The organic matter types are mainly types II_1 and II_2. The simulations of hydrocarbon generation and expulsion suggest

that E_2L_{2X} in the deep syncline to the north of the Meihua Fault has initiated the expulsion of hydrocarbons, whereas other regions remain inactive. The Huangtong Sag marks the initial phase of hydrocarbon expulsion, succeeded by the Bailian Sag, with the Huachang Sub-uplift experiencing the latest expulsion. Source rocks reach the hydrocarbon expulsion threshold at 2700 m, with peak generation at 2370 m (510 mg/g) and peak expulsion at 3220 m (430 mg/g). The maximum expulsion efficiency is 88%. The expulsion thresholds for E_2L_1, E_2L_2, and E_2L_3 are 2650, 2720, and 2640 m, with peaks at 3170, 3380, and 3600 m, respectively, all above an efficiency of 84%. The hydrocarbon generation and expulsion centers of E_2L_1 and E_2L_2 are in the Guangdong and Bailian Sags, while the centers of E_2L_3 are in Huangtong, Bailian, and Huachang. The prospective resources of E_2L_2 in the Fushan Depression hold 14.92×10^8 tons (75.46% of total resources), making it the main source rock, compared with 20.46% of E_2L_1 and 4.08% of E_2L_3.

Author Contributions: Conceptualization, X.W. and F.J.; methodology, X.W. and X.Z.; software, Z.Q., J.G. and Y.Z.; validation, X.W. and F.J.; formal analysis, X.W. and D.C.; investigation, X.W. and D.C.; resources, F.J.; data curation, Y.L. and J.G.; writing—original draft, X.W.; writing—review and editing, X.W. and X.Z.; visualization, X.W.; supervision, F.J.; project administration, X.W.; funding acquisition, F.J. All authors have read and agreed to the published version of the manuscript.

Funding: This study was supported by the National Natural Science Foundation of China [Grant No: 42372147].

Data Availability Statement: The data are contained within this article.

Conflicts of Interest: The authors declare no conflicts of interest.

References

1. Huang, B.; Tian, H.; Wilkins, R.; Xiao, X.; Li, L. Geochemical characteristics, palaeoenvironment and formation model of Eocene organic-rich shales in the Beibuwan Basin, South China Sea. *Mar. Pet. Geol.* **2013**, *48*, 77–89. [CrossRef]
2. Huang, B.; Xiao, X.; Cai, D.; Wilkins, R.; Liu, M. Oil families and their source rocks in the Weixinan Sub-basin, Beibuwan Basin, South China Sea. *Org. Geochem.* **2011**, *42*, 134–145. [CrossRef]
3. Li, Y.; Li, L.; Wang, K.; Yang, Y. Differences in lacustrine source rocks of Liushagang Formation in the Beibuwan Basin. *Acta Pet. Sin.* **2019**, *40*, 1451.
4. Li, C.; Zhang, G.; Liang, J.; Zhao, Z.; Xu, J. Characteristics of fault structure and its control on hydrocarbons in the Beibuwan Basin. *Acta Pet. Sin.* **2012**, *33*, 195–203.
5. Deng, Y.; Peng, H.L.; Pei, J.X.; He, J.W.; Shi, D.F. De-ghosting method based on seismic wavelet derived from water-bottom in marine seismic data. *Prog. Geophys.* **2020**, *35*, 281–286.
6. Li, S.; Lin, C.; Zhang, Q.; Yang, S.; Wu, P. Episodic rifting of continental marginal basins and tectonic events since 10 Ma in the South China Sea. *Chin. Sci. Bull.* **1999**, *44*, 10–23. [CrossRef]
7. Liu, E.; Wang, H.; Li, Y.; Zhou, W.; Leonard, N.D.; Lin, Z.; Ma, Q. Sedimentary characteristics and tectonic setting of sublacustrine fans in a half-graben rift depression, Beibuwan Basin, South China Sea. *Mar. Pet. Geol.* **2014**, *52*, 9–21. [CrossRef]
8. Deng, Y.; Hu, D.; Zhu, J.; Liu, G.; Chen, K.; Tong, C.; Zhang, D.; Xu, X.; Man, Y.; You, J.; et al. Hydrocarbon accumulation regularities, new fields and new types of exploration, and resource potentials in Beibuwan Basin. *Acta Pet. Sin.* **2024**, *45*, 202.
9. Fu, N.; Lin, Q.; Wang, K. Main source rock reevaluation of Member 2 of Liushagang Formation in the sags of Beibuwan basin. *China Offshore Oil Gas* **2017**, *29*, 12–21.
10. Liu, Y.; Ren, Y.J.; Yang, X.B.; Liu, H.; Xu, X. Geochemical Signatures of the Source Rocks from the Liushagang Formation in the Wushi Depression, Beibuwan Basin. *Sediment. Geol. Tethyan Geol.* **2018**, *38*, 103–112.
11. Luo, Q.; Pang, X. Reservoir controlling mechanism and petroleum accumulation model for consequent fault and antithetic fault in Fushan Depression of Hainan area. *Acta Pet. Sin.* **2008**, *29*, 363.
12. Xie, R.; Huang, B.; Li, X. Hydrocarbon generation potential evaluation of source rocks in Liushagang Formation in Weixinan Sag of Beibuwan Basin. *J. Geol.* **2014**, *38*, 670–675.
13. Gan, H.; Wang, H.; Shi, Y.; Ma, Q.; Liu, E.; Yan, D.; Pan, Z. Geochemical characteristics and genetic origin of crude oil in the Fushan sag, Beibuwan Basin, South China Sea. *Mar. Pet. Geol.* **2020**, *112*, 104114. [CrossRef]
14. Huang, B.; Zhu, W.; Tian, H.; Jin, Q.; Xiao, X.; Hu, C. Characterization of Eocene lacustrine source rocks and their oils in the Beibuwan Basin, offshore South China Sea. *Aapg Bull.* **2017**, *101*, 1395–1423. [CrossRef]
15. Li, M.; Wang, T.; Liu, J.; Lu, H.; Wu, W.; Gao, L. Occurrence and origin of carbon dioxide in the Fushan depression, Beibuwan Basin, South China Sea. *Mar. Pet. Geol.* **2008**, *25*, 500–513. [CrossRef]
16. Hu, L.; Jin, Q.; Yang, X.; Hu, D.; Lu, M. Structure evolution and middle-shallow hydrocarbon enrichment patters in the eastern Wushi Sag. *Spec. Oil Gas Reserv.* **2020**, *27*, 68.

17. Fu, N.; Wang, K.; Jia, Q.J. Formation of oil and gas in the Fushan sag of Beibuwan Basin under the co-control of source and heat. *Acta Pet. Sin.* **2019**, *40*, 38–45.
18. Yan, S.; Li, Y.; Wu, Z.; Yang, X.; Hu, L. Structure characteristics and genetic mechanism of Haizhong sag and Weixinan sag in Beibu gulf basin. *Acta Pet. Sin.* **2020**, *41*, 711.
19. Zhu, W. Relations between fractures and hydrocarbon reservoirs in Weixinan sag. *Acta Pet. Sin.* **1998**, *19*, 6.
20. Chen, S.; Gan, H.; Shi, Y.; Zhao, Y.; Wang, X. Geochemical features and geologic significance of source rocks in Fushan Sag, Beibuwan Basin. *Pet. Geol. Recovery Effic.* **2015**, *22*, 14–19.
21. Zhao, Y.; Gan, H.; Shi, Y.; Chen, S.; Wang, G. Characteristics of geothermal anomaly and its effect on oil and gas reservoir in Fushan sag of Beibuwan Basin. *Pet. Geol. Recovery Effic.* **2016**, *23*, 40–46. [CrossRef]
22. Hu, T.; Pang, X.; Jiang, F.; Zhang, C.; Wu, G.; Hu, M.; Jiang, L.; Wang, Q.; Xu, T.; Hu, Y. Dynamic continuous hydrocarbon accumulation (DCHA): Existing theories and a new unified accumulation model. *Earth-Sci. Rev.* **2022**, *232*, 104109. [CrossRef]
23. Hanson, A.D.; Ritts, B.D.; Moldowan, J.M. Organic geochemistry of oil and source rock strata of the Ordos Basin, north-central China. *AAPG Bull.* **2007**, *91*, 1273–1293. [CrossRef]
24. Peters, K.E. Guidelines for evaluating petroleum source rock using programmed pyrolysis. *AAPG Bull.* **1986**, *70*, 318–329.
25. Peters, K.E.; Cassa, M.R. Applied Source Rock Geochemistry: Chapter 5: Part II. Essential Elements. In *The Petroleum System: From Source to Trap*; Magoon, L.B., Dow, W.G., Eds.; American Association of Petroleum Geologists: Tulsa, OK, USA, 1994; pp. 93–120.
26. Tissot, B.P.; Welte, D.H. *Petroleum Formation and Occurrence*; Springer Science & Business Media: Berlin/Heidelberg, Germany, 2013.
27. Wu, M.; Cao, J.; Wang, X.; Tang, Y.; Wang, B.; Xiang, B.; Kang, S.; Lan, W. Hydrocarbon generation potential of Triassic mudstones in the Junggar Basin, northwest China. *AAPG Bull.* **2014**, *98*, 1885–1906. [CrossRef]
28. Hunt, J.M. Generation of gas and oil from coal and other terrestrial organic matter. *Org. Geochem.* **1991**, *17*, 673–680. [CrossRef]
29. Hazra, B.; Dutta, S.; Kumar, S. TOC calculation of organic matter rich sediments using Rock-Eval pyrolysis: Critical consideration and insights. *Int. J. Coal Geol.* **2017**, *169*, 106–115. [CrossRef]
30. Hazra, B.; Karacan, C.Ö.; Tiwari, D.M.; Singh, P.K.; Singh, A.K. Insights from Rock-Eval analysis on the influence of sample weight on hydrocarbon generation from Lower Permian organic matter rich rocks, West Bokaro basin, India. *Mar. Pet. Geol.* **2019**, *106*, 160–170. [CrossRef]
31. Karayigit, A.I.; Oskay, R.G.; Çelik, Y. Mineralogy, petrography, and Rock-Eval pyrolysis of late Oligocene coal seams in the Malkara coal field from the Thrace Basin (NW Turkey). *Int. J. Coal Geol.* **2021**, *244*, 103814. [CrossRef]
32. Vu, T.T.A.; Horsfield, B.; Mahlstedt, N.; Schenk, H.J.; Kelemen, S.R.; Walters, C.C.; Kwiatek, P.J.; Sykes, R. The structural evolution of organic matter during maturation of coals and its impact on petroleum potential and feedstock for the deep biosphere. *Org. Geochem.* **2013**, *62*, 17–27. [CrossRef]
33. Yang, S.; Horsfield, B. Critical review of the uncertainty of Tmax in revealing the thermal maturity of organic matter in sedimentary rocks. *Int. J. Coal Geol.* **2020**, *225*, 103500. [CrossRef]
34. Kleijnen, J.P. *Design and Analysis of Simulation Experiments*; Springer: Berlin/Heidelberg, Germany, 2018.
35. Kovács, G. *Seepage Hydraulics*; Elsevier: Amsterdam, The Netherlands, 2011.
36. Pang, X.; Chen, Z.; Chen, F. Basic concept of hydrocarbon expulsion threshold and its research significance and application. *Geoscience* **1997**, *11*, 510–521.
37. Sandvik, E.I.; Young, W.A.; Curry, D.J. Expulsion from hydrocarbon sources: The role of organic absorption. *Org. Geochem.* **1992**, *19*, 77–87. [CrossRef]
38. Hammes, U.; Hamlin, H.S.; Ewing, T.E. Geologic analysis of the Upper Jurassic Haynesville Shale in east Texas and west Louisiana. *AAPG Bull.* **2011**, *95*, 1643–1666. [CrossRef]
39. Klemme, H.D.; Ulmishek, G.F. Effective petroleum source rocks of the world: Stratigraphic distribution and controlling depositional factors (1). *AAPG Bull.* **1991**, *75*, 1809–1851.
40. Welte, D.H. Relation between petroleum and source rock. *AAPG Bull.* **1965**, *49*, 2246–2268.
41. Stainforth, J.G.; Reinders, J. Primary migration of hydrocarbons by diffusion through organic matter networks, and its effect on oil and gas generation. *Org. Geochem.* **1990**, *16*, 61–74. [CrossRef]
42. Brenneman, M.C.; Smith, P.V., Jr. The Chemical Relationships between Crude Oils and Their Source Rocks: Topical Papers. In *SP 18: Habitat of Oil*; WEEKS, L.G., Ed.; American Association of Petroleum Geologists: Tulsa, OK, USA, 1958; pp. 818–849.
43. Lewan, M.D.; Winters, J.C.; McDonald, J.H. Generation of oil-like pyrolyzates from organic-rich shales. *Science* **1979**, *203*, 897–899. [CrossRef]
44. Ma, Q.L.; Zhao, S.E.; Liao, Y.T.; Lin, Z.L. Sequence architectures of Paleogene Liushagang Formation and its significance in Fushan Sag of the Beibuwan Basin. *Earth Sci.-J. China Univ. Geosci.* **2012**, *37*, 667–678.
45. Shi, Y.M.; Liu, J.; Zhang, M.Z.; Chen, D.; Ma, Q. Experience and understand in oil and gas exploration in Fushan Sag, Hainan Province. *South China J. Seismol.* **2007**, *27*, 57–68.
46. Wang, S.-H.; Li, Z.; Zhou, W.; Huan, Y.-L.; Liu, Q.; Xu, X.-Y. A preliminary study on petroleum accumulation in the Qom Basin, Iran. *Exp. Pet. Geol.* **2004**, *26*, 236–240.
47. Liao, F.; Zen, W.; Lu, Z.; Chen, G.; Shi, H.; Long, Z.; Shi, Y. Study of lithologic reservoir of Paleogene Liushagang Formation in Fushan depression of Beibu Bay Basin. *China Pet. Explor.* **2015**, *20*, 43.
48. Wei, C.G.; He, Y.D.; Geng, C.B. Faulting Mechanism in Northern Depression of the Beibuwan Basin, China. *Geotecton. Et Metallog.* **2008**, *32*, 28–35.

49. Zhao, Y.D.; Wang, H.; Gan, H.J.; Chen, S.B.; Wang, X. The analysis about evolution of basin morphology in Fushan sag of Hainan province. *J. China Univ. Min. Technol.* **2014**, *43*, 1078–1086.
50. Jin, S.; Wang, H.; Cao, H.; Chen, S.; Lin, Z.; Yu, J.; Pan, S. Sedimentation of the paleogene liushagang formation and the response to regional tectonics in the fushan sag, beibuwan basin, south china sea. *Austrian J. Earth Sci.* **2014**, *107*, 112–130.
51. Li, Y.; Wang, H.; Zhang, G.; Lin, S. Depositional evolution and models for a deep-lacustrine gravity flow system in a half-graben rifted sag, Beibuwan Basin, South China Sea. *Geol. Acta Int. Earth Sci. J.* **2022**, *20*, 3. [CrossRef]
52. Wang, G.; Wang, H.; Gan, H.; Liu, E.; Xia, C.; Zhao, Y.; Chen, S.; Zhang, C. Paleogene tectonic evolution controls on sequence stratigraphic patterns in the Fushan sag, northern South China Sea. *J. Earth Sci.* **2016**, *27*, 654–669. [CrossRef]
53. Wang, P.; Li, S.; Suo, Y.; Guo, L.; Santosh, M.; Li, X.; Wang, G.; Jiang, Z.; Liu, B.; Zhou, J. Structural and kinematic analysis of Cenozoic rift basins in South China Sea: A synthesis. *Earth-Sci. Rev.* **2021**, *216*, 103522. [CrossRef]
54. Jin, S.; Wang, H.; Cao, H.; Gan, H.; Chen, S. Lake-type controls on sedimentary infill and petroleum source rocks in the Palaeogene Fushan Depression, Beibuwan Basin, South China. *Geol. J.* **2020**, *55*, 3936–3956. [CrossRef]
55. Lu, Y.; Li, M.; Wang, T.; Shi, Y. Dibenzothiophenes and benzonaphthothiophenes in oils, and their application in identifying oil filling pathways in Eocene lacustrine clastic reservoirs in the Beibuwan Basin, South China Sea. *J. Pet. Sci. Eng.* **2016**, *146*, 1026–1036.
56. Zhang, G.; Zhang, Y.; Shen, H.; He, Y. An analysis of natural gas exploration potential in the Qiongdongnan Basin by use of the theory of "joint control of source rocks and geothermal heat". *Nat. Gas Ind. B* **2014**, *1*, 41–50.
57. Zeng, B.; Li, M.; Zhu, J.; Wang, X.; Shi, Y.; Zhu, Z.; Guo, H.; Wang, F. Selective methods of TOC content estimation for organic-rich interbedded mudstone source rocks. *J. Nat. Gas Sci. Eng.* **2021**, *93*, 104064. [CrossRef]
58. Liu, E.; Wang, H.; Feng, Y.; Pan, S.; Jing, Z.; Ma, Q.; Gan, H.; Zhao, J. Sedimentary architecture and provenance analysis of a sublacustrine fan system in a half-graben rift depression of the South China Sea. *Sediment. Geol.* **2020**, *409*, 105781. [CrossRef]
59. Jin, Z.; Wang, J.; Zhang, S.; Wang, J.; Zhang, F. Main factors controlling hydrocarbon reservoirs and exploration directions in the pre-salt sequence in Precaspian Basin. *Pet. Geol. Exp.* **2007**, *29*, 111.
60. Liu, L.-J.; Tong, Y.-M.; Ji, Y.-L.; Kuang, H.-W.; Lu, M.-G. Sedimentary characteristics and developing background of the sublacustrine fan in the Liushagang Formation of the Fushan depression, the Beibuwan Basin. *Exp. Pet. Geol.* **2003**, *25*, 110–115.
61. Fu, C.; Yu, X.; Chen, W.; Ren, G.; Liu, D. Strata Architectural Variability and Facies Distribution in a Structural Transfer Zone: A Case Study of Fushan Sag, Northern South China Sea. *Acta Geol. Sin.-Engl. Ed.* **2021**, *95*, 1998–2015. [CrossRef]
62. Xiu, L. Classifications and establishment of SPE reserve. *China Pet. Explor.* **2010**, *15*, 52.
63. Espitalié, J.; Laporte, J.L.; Madec, M.; Marquis, F.; Leplat, P.; Paulet, J. Méthode rapide de caractérisation des roches mètres, de leur potentiel pétrolier et de leur degré d'évolution. *Rev. Inst. Fr. Pét.* **1977**, *32*, 23–43. [CrossRef]
64. Carvajal-Ortiz, H.; Gentzis, T.; Ostadhassan, M. Sulfur differentiation in organic-rich shales and carbonates via open-system programmed pyrolysis and oxidation: Insights into fluid souring and H2S production in the Bakken Shale, USA. *Energy Fuels* **2021**, *35*, 12030–12044. [CrossRef]
65. Alexandridis, I.; Oikonomopoulos, I.K.; Carvajal-Ortiz, H.; Gentzis, T.; Kalaitzidis, S.; Georgakopoulos, A.; Christanis, K. Discovery of a new source-rock interval within the Pantokrator Formation, Ionian Zone, western Greece: Insights from sulfur speciation and kinetics analyses. *Mar. Pet. Geol.* **2022**, *145*, 105918. [CrossRef]
66. *ISO 7404-2*; Methods for the Petrographic Analysis of Coals—Part 2: Methods of Preparing Coal Samples. International Organization for Standardization: Geneva, Switzerland, 2009. Available online: www.iso.org/standard/42798.html (accessed on 22 September 2024).
67. *ISO 7404-5*; Methods for the Petrographic Analysis of Coals—Part 5: Method of Determining Microscopically the Reflectance of Vitrinite. International Organization for Standardization: Geneva, Switzerland, 2009. Available online: www.iso.org/standard/42832.html (accessed on 22 September 2024).
68. *ASTM D7708-14*; Standard Test Method for Microscopical Determination of the Reflectance of Vitrinite Dispersed in Sedimentary Rocks. ASTM International: West Conshohocken, PA, USA, 2014. Available online: www.astm.org (accessed on 22 September 2024).
69. Huang, D. *Advances in Hydrocarbon Generation Theory (I)—Immature Oils and Generating Hydrocarbon and Evolutionary Model, Geology of Fossil Fuels—Oil and Ga*; CRC Press: Boca Raton, FL, USA, 2021; pp. 3–15.
70. Pang, X.; Li, M.; Li, S.; Jin, Z. Geochemistry of petroleum systems in the Niuzhuang South Slope of Bohai Bay Basin: Part 3. Estimating hydrocarbon expulsion from the Shahejie formation. *Org. Geochem.* **2005**, *36*, 497–510. [CrossRef]
71. Cooles, G.P.; Mackenzie, A.; Quigley, T.M. Calculation of petroleum masses generated and expelled from source rocks. *Org. Geochem.* **1986**, *10*, 235–245. [CrossRef]
72. Jin, Q. The restoration of initial organic carbon in source rocks. *J. Univ. Pet. China* **1989**, *13*, 1–8.
73. Guo, J.; Pang, X.; Guo, F.; Wang, X.; Xiang, C.; Jiang, F.; Wang, P.; Xu, J.; Hu, T.; Peng, W. Petroleum generation and expulsion characteristics of Lower and Middle Jurassic source rocks on the southern margin of Junggar Basin, northwest China: Implications for unconventional gas potential. *Can. J. Earth Sci.* **2014**, *51*, 537–557. [CrossRef]
74. Dembicki, H., Jr. Three common source rock evaluation errors made by geologists during prospect or play appraisals. *AAPG Bull.* **2009**, *93*, 341–356. [CrossRef]
75. Li, M.; Wang, T.; Liu, J.; Zhang, M.; Lu, H.; Ma, Q.; Gao, L. The occurrence of oleananes in the Beibuwan Basin and its application to the study of maturity and oil-source rock correlation. *Acta Geol. Sin.-Engl. Ed.* **2008**, *82*, 585–595.

76. Liu, E.; Wang, H.; Li, Y.; Leonard, N.D.; Feng, Y.; Pan, S.; Xia, C. Relative role of accommodation zones in controlling stratal architectural variability and facies distribution: Insights from the Fushan Depression, South China Sea. *Mar. Pet. Geol.* **2015**, *68*, 219–239. [CrossRef]
77. Zeng, B.; Li, M.; Wang, X.; Wang, F.; Gong, C.; Lai, J.; Shi, Y. Source rock evaluation within a sequence stratigraphic framework of the Palaeogene Liushagang Formation in the Fushan Depression, South China Sea. *Geol. J.* **2022**, *57*, 2409–2427. [CrossRef]
78. Li, Y.; Lin, S.; Wang, H.; Luo, D. Depositional setting analysis using seismic sedimentology: Example from the Paleogene Lishagang sequence in the Fushan depression, South China Sea. *Geod. Geodyn.* **2017**, *8*, 347–355. [CrossRef]